KUOPION YLIOPISTON JULKAISUJA G. - A.I. VIRTANEN -INSTITUUTTI 2
KUOPIO UNIVERSITY PUBLICATIONS G.
A.I. VIRTANEN INSTITUTE FOR MOLECULAR SCIENCES 2

MIKKO KETTUNEN

A Study of Magnetic Resonance Imaging Contrast Generation and Pathophysiology in Acute Cerebral Ischaemia

Doctoral dissertation

To be presented by permission of the Faculty of Natural and Environmental Sciences of the University of Kuopio for public examination in Auditorium L22, Snellmania building, University of Kuopio, on Wednesday 19th June 2002, at 12 noon

Department of Biomedical NMR and National Bio-NMR Facility
A.I. Virtanen Institute for Molecular Sciences
University of Kuopio

KUOPION YLIOPISTO
KUOPIO 2002

Distributor:

Kuopio University Library
P.O.Box 1627
FIN-70211 KUOPIO
FINLAND
Tel. +358 17 163 430
Fax +358 17 163 410

Series editors:

Professor Karl Åkerman
Department of Neurobiology
A.I. Virtanen Institute

Jarmo Wahlfors
Department of Biotechnology and Molecular Medicine
A.I. Virtanen Institute

Author´s address:

Department of Biomedical NMR and National Bio-NMR Facility
A.I. Virtanen Institute for Molecular Sciences
University of Kuopio
P.O.Box 1627
FIN-70211 KUOPIO
FINLAND
Tel. +358 17 162 023
Fax +358 17 163 030

Supervisors:

Professor Risto Kauppinen, M.D., Ph.D.
Department of Biomedical NMR
A.I. Virtanen Institute

Olli Gröhn, Ph.D.
Department of Biomedical NMR
A.I. Virtanen Institute

Reviewers:

Professor Roger Ordidge, Ph.D.
Department of Medical Physics & Bioengineering
University College
London, UK

Docent Turgut Tatlisumak, M.D., Ph.D.
Department of Neurology
Helsinki University Central Hospital
Finland

Opponent:

Professor David Gadian, Ph.D.
Radiology and Physics Unit
Institute of Child Health
London, UK

ISBN 951-781-961-7
ISSN 1458-7335

Kuopio University Printing Office
Kuopio 2002
Finland

Kettunen, Mikko. A Study of Magnetic Resonance Imaging Contrast Generation and Pathophysiology in Acute Cerebral Ischaemia. Kuopio University Publications G. - A.I. Virtanen Institute for Molecular Sciences 2. 2002. 67 p.
ISBN 951-781-961-7
ISSN 1458-7335

Abstract

Magnetic resonance imaging (MRI) allows non-invasive assessment of tissue and haemodynamic status during and after cerebral ischaemia, making it the method of choice for detecting acute ischaemia in experimental and clinical settings. In this work, immediate responses of MRI relaxation times T_1, $T_{1\rho}$ and T_2 to hyperacute cerebral ischaemia were examined in rat models mainly at 4.7 T with the aim of distinguishing between the haemodynamic and tissue alterations to MRI in the ischaemic brain. The contributions of cerebral blood flow (CBF) on T_1, chemical exchange on $T_{1\rho}$ and a blood oxygen saturation level (BOLD) effect on T_2 were the main focus of this study.

It was observed that T_1 prolongs within seconds after the onset of global ischaemia, preceding the decline in water diffusion. A similar T_1 increase was detected also at 1.5 T, indicating that the phenomenon is detectable at clinical field strengths. In transient middle cerebral artery occlusion (MCAO), elevated T_1 was observed within 10 minutes, well before the net water accumulation into the tissue. Cerebral T_1 either remained elevated or partially recovered upon retraction of the occluder thread. Interestingly, in the former case, diffusion did not normalise, but in the latter case it fully recovered. The early T_1 change is mainly attributed to direct effects from the cessation of blood flow.

Similarly to T_1, prolonged $T_{1\rho}$ was observed earlier than the decline in diffusion of tissue water in global ischaemia. The kinetics of $T_{1\rho}$ proceeded independently of anoxic depolarisation and were not influenced by the pre-ischaemic blood glucose level. The data suggest that the early $T_{1\rho}$ increase is not directly caused by CBF or ionic and/or water shifts across the cell membrane associated with anoxic depolarisation. In contrast, the steady-state $T_{1\rho}$ positively correlates with ischaemic lactate concentration. This is consistent with the pH dependency of $T_{1\rho}$ that was shown to prevail in the energetically viable brain tissue. *In vitro* $T_{1\rho}$ demonstrated sensitivity to susceptibility effects from blood oxygen saturation and dissolved O_2, yet *in vivo* the effects appeared to be of minor importance.

Shortening of single Hahn echo T_2, associated with acute ischaemia, was assigned to a negative intravascular BOLD effect. The contributions of CBF, cerebral blood volume and oxygen extraction ratio (OER) to the positive post-ischaemic T_2 BOLD were also studied. The data highlight the significant contribution of low OER due to depressed oxygen metabolism, indicating that metabolic, rather than haemodynamic factors may dominate post-ischaemic BOLD MRI.

These results challenge the conventional concept of delayed MR relaxation responses by demonstrating substantial changes in T_1, $T_{1\rho}$ and T_2 in the cerebral parenchyma during hyperacute ischaemia. Haemodynamic and tissue contributions to these relaxation parameters are assigned, and it is shown, that while the former factor is a key substrate for the T_1 and T_2 changes, $T_{1\rho}$ reveals a genuine change in the physico-chemical microenvironment of brain tissue.

National Library of Medicine Classification: WN 185, WL 355, WG 106
Medical Subject Headings: magnetic resonance imaging; magnetic resonance spectroscopy; brain; brain ischemia / diagnosis; brain ischemia / physiopathology; oxygen / metabolism; cerebrovascular circulation; hemodynamics; rats

Acknowledgements

This study was carried out in the A. I. Virtanen Institute for Molecular Sciences, University of Kuopio, during the years 1998-2002.

I express my gratitude to my principal supervisor, Professor Risto Kauppinen, M.D. Ph.D., for offering me the chance to work in his laboratory during these years as well as for his optimism and inspiration. His endless dedication to scientific work has formed the backbone of this work.

I am grateful to my other supervisor, Olli Gröhn, Ph.D., for his significant contribution in the experimental parts of this study as well as for the many stimulating conversations and valuable insight into the different aspects of MRI of cerebral ischaemia.

I thank the official reviewers, Professor Roger Ordidge, Ph.D., and Docent Turgut Tatlisumak, M.D., for their evaluation and constructive criticism of this work. I also thank Ewan Macdonald, Ph.D., for revising the language of the manuscript.

No experimental study is possible without a group of skillful co-workers. I am grateful to Docent Markku Penttonen, Ph.D., for his expertise in electrophysiology. My thanks also go to Johanna Närväinen, M.Sc., for her help in mathematical simulations as well as for contributing many valuable ideas and explanations during these years. I am indebted to Niina Kuhmonen, Jouko Lukkarinen, Ph.D., and Kati Holopainen for their expert technical assistance, and to Martin Kavec, Dipl. Ing., for his skillful design, construction and repair of the rf-coils used in the study. My thanks also go to Juhana Hakumäki, M.D., Ph.D., Heidi Mäkelä, M.Sc., and all the other members of the NMR Research Group at the A.I. Virtanen Institute, who have contributed countless hours of technical assistance, new ideas and valuable criticism to this work. I am grateful to Pauli Vainio, Ph.L., for his help with MRI at clinical settings, and to Kari Mauranen, M.Sc., for his advice on statistical analysis.

I am deeply grateful to my parents, Leena and Jussi Kettunen, and my brothers, Ville and Juho, who have always provided advice, encouragement and support.

This study was financially supported by the Northern Savo Fund of Finnish Cultural Foundation, the Aarne and Aili Turunen Foundation, the Magnus Ehrnrooth Foundation, the Academy of Finland and the Sigrid Juselius Foundation. AMI-227 was a kind donation from Guerbet, France.

Kuopio, June 2002

Mikko Kettunen

Abbreviations

ADC	apparent diffusion coefficient
ASL	arterial spin labeling
ATP	adenosine triphosphate
B_0 field	main magnetic field
B_1, B_2 field	radio-frequency field
BOLD	blood oxygen level dependent
BSA	bovine serum albumin
CBF	cerebral blood flow
CBV	cerebral blood volume
$CMRO_2$	cerebral metabolic rate of oxygen
CCA	common carotid artery
CP	Carr-Purcell multi-echo
CPMG	Carr-Purcell-Meiboom-Gill multi-echo
CPP	cerebral perfusion pressure, cerebral perfusion pressure
D	diffusion coefficient
D_{av}	1/3 of the trace of the diffusion tensor
DSC-MRI	dynamic susceptibility contrast magnetic resonance imaging, "perfusion imaging"
$d_{T1\rho}$	B_1 field dependency of $T_{1\rho}$, $T_{1\rho}$ dispersion
ECS	extracellular space
EPI	echo-planar imaging
FLASH	fast low angle shot imaging
GRE	gradient echo
γ	gyromagnetic ratio
i.p.	intraperitoneally
i.v.	intravenously
IR	inversion recovery
LASER	localization by adiabatic selective refocusing
MABP	mean arterial blood pressure
MCA	middle cerebral artery
MCAO	middle cerebral artery occlusion
M	net magnetisation vector, signal intensity
M_0	steady-state magnetisation
M_{sat}	magnetisation in the presence of off-resonance B_2 field
MRA	magnetic resonance angiography
MRI	magnetic resonance imaging
MRS	magnetic resonance spectroscopy

MRUI	Magnetic Resonance User Interface
MT	magnetisation transfer
MTR	magnetisation transfer ratio
MTT	mean transit time
NAA	N-acetyl aspartate
NMR	nuclear magnetic resonance
OER	oxygen extraction ratio
PCr	phosphocreatine
pH_i	intracellular pH
P_i	inorganic phosphate
PtO_2	tissue oxygen tension
$\Delta\omega$	magnetic susceptibility difference
R_1	longitudinal relaxation rate ($1/T_1$)
R_2	transverse relaxation rate ($1/T_2$)
rf	radio-frequency
SAR	specific absorption rate of energy
SE	spin-echo
SLT	spin-lock time
T_1	longitudinal relaxation time
$T_{1\rho}$	longitudinal relaxation time in the rotating frame
T_2	transverse relaxation time
T_2^*	effective transverse relaxation time, including signal reduction from the incoherent dephasing effect caused by diffusion through field gradients plus coherent dephasing effects from local field inhomogeneities and susceptibility differences
τ_{CPMG}	delay for a echo refocusing in a CPMG experiment
TE	time to echo, “echo time”
TI	time from inversion, "inversion time"
TR	time to repeat, “repetition time”
x_{deoxy}	fraction of deoxygenated haemoglobin
Y_a	arterial oxygenation fraction

List of original publications

This dissertation is based on the following papers referred to by their corresponding Roman numerals:

I Kettunen MI, Gröhn OHJ, Lukkarinen JA, Vainio P, Silvennoinen MJ and Kauppinen RA. Interrelations of T_1 and Diffusion of Water in Acute Cerebral Ischaemia of the Rat. Magn Reson Med 2000;44:833-839.

II Kettunen MI, Gröhn OHJ, Silvennoinen MJ, Penttonen M and Kauppinen RA. Effects of Intracellular pH, Blood, and Tissue Oxygen Tensions on the $T_{1\rho}$ Relaxation in the Rat Brain. 2002, submitted.

III Kettunen MI, Gröhn OHJ, Penttonen M and Kauppinen RA. Cerebral $T_{1\rho}$ Relaxation Time Increases Immediately Upon Global Ischaemia in the Rat Independently of Blood Glucose And Anoxic Depolarization. Magn Reson Med 2001;46:565-572.

IV Kettunen MI, Gröhn OHJ, Silvennoinen MJ, Penttonen M and Kauppinen RA. Quantitative Assessment of the Balance Between Oxygen Delivery and Consumption in the Rat Brain Following Transient Ischaemia by T_2-BOLD MRI. J Cereb Blood Flow Metab 2002;22:262-270.

Table of contents

1 INTRODUCTION

Cerebrovascular disease is one of the leading causes of mortality and morbidity in the western world. Acute cerebral ischaemia, commonly termed ischaemic stroke, is the most common form of cerebrovascular disease (235). Recent advances in treatment protocols have emphasised the importance of early and accurate diagnosis of stroke (3, 12, 77, 83, 148). Magnetic resonance imaging (MRI) is an invaluable tool for imaging of acute brain conditions including acute ischaemic stroke (12, 16, 181) since pathophysiologic alterations associated with compromised cerebral haemodynamics cause changes in the biophysical properties of water, making it possible to delineate ischaemia and monitor its evolution.

In the clinical settings, diffusion MRI, complemented with T_2-weighted or perfusion MRI, has paved new avenues for the assignment of ischaemia, thus aiding in decision making for "targeted" treatment of brain tissue. The MRI methods currently provide a framework for imaging of acute brain ischaemia, since diffusion detects energy failure (168), T_2 hyperintensity is a well-documented signature of irreversible ischaemia (240) and the status of cerebral haemodynamics can be revealed by perfusion imaging (12).

The MRI repertoire for the assessment of brain tissue viability and status has recently been complemented by demonstrations in experimental stroke models that both T_1 and T_2 change soon after the collapse of blood supply to the brain (35, 46, 48, 88, 89). These observations have challenged the "traditional" interpretation of MRI in acute ischaemia, arguing that the net water accumulation into irreversibly damaged tissue is the key pathophysiologic factor underlying these contrasts. The recent data suggest that cessation of cerebral blood flow (CBF) may be a significant factor to T_1 contrast in ischaemic brain (35, 155). Blood oxygen level dependent (BOLD) effect has been ascribed to the shortening of both T_2 and T_2* in acute ischaemia (35, 46, 48, 88, 89, 202). The demonstration of the BOLD effect in conjunction with compromised CBF is particularly interesting, since it links the MRI contrast directly to the tissue metabolism thus allowing for "imaging" of residual oxidative activity (86, 88, 155). It can be anticipated that substantial insight into the pathophysiology of acute ischaemia will become available through quantitative T_1 and T_2 MRI.

Gröhn et al. recently demonstrated that the T_1 in the rotating frame ($T_{1\rho}$) is prolonged in the early moments of focal ischaemia of rat (90) and that the $T_{1\rho}$ contrast afforded by the MRI data obtained with multiple spin-lock fields, so called $T_{1\rho}$ dispersion, extensively changes within minutes of the insult (87). It was also shown that quantitative $T_{1\rho}$ MRI was able to delineate irreversible ischaemia in a transient focal ischaemia model (87). The CBF threshold yielding $T_{1\rho}$ and diffusion contrasts was found to be ~20 ml/100g/min, suggesting that reduced aerobic metabolism and ischaemia with exhausted chemical energy are required for expression of cerebral $T_{1\rho}$ contrast. $T_{1\rho}$ relaxation is expected to probe the interactions taking place at the water-protein-interface. However, to date, the pathophysiological mechanisms contributing to the $T_{1\rho}$ relaxation in tissue have only been partially characterised.

2 REVIEW OF THE LITERATURE

2.1 Preface

The framework for the present study comprises application of advanced MRI technology to the assessment of consequences of acute cessation of blood supply to the brain. In the following section, a brief introduction to the imaging methodology as well as to the known pathophysiology of various forms of brain ischaemia is given.

2.2 Nuclear magnetic resonance (NMR)

Nuclear magnetic resonance (NMR) arises from the physical properties of a nucleus. The nucleus possesses a quantised vector property called the nuclear spin angular momentum, spin, I, with values of 0, ½, 1 and so on depending on the number of protons and neutrons in a given nucleus. Nuclei with spin values different from zero interact with the external magnetic field thus enabling the detection of the NMR signal. The two most commonly used nuclei for *in vivo* NMR, ^{1}H and ^{31}P, have I=½. The choice of these atoms for biological NMR is understandable, since on one hand, the natural abundance of these two atoms is close to 100% and on the other, molecules containing high quantities of ^{1}H and ^{31}P are present in the body. The ^{1}H (a proton) nucleus is used as an example of an NMR visible nucleus in the following theory section. It should be noted, however, that although many of the basic concepts of NMR can be presented using classical formalism, a fundamental description of NMR would require a treatment using quantum mechanics and principles of statistical mechanics. A more detailed description of NMR can be found in several textbooks (1, 63, 72, 79).

2.2.1 Magnetisation

"Magnetisation" is a commonly used term in the literature to describe pulsed NMR experiments and stands for the x, y or z component of angular moment operators I_x, I_y or I_z. In the earth's weak magnetic field, the spins are randomly oriented so that the net sum of vectors, the net magnetisation M, is virtually zero. When a sample is placed into a strong external magnetic field, referred to as a B_0 field, the spins align to 2I+1 different orientations, with different energy levels dependent on the B_0 field. This means that protons are aligned either against (-½) or along (½) the B_0 field according to the Boltzmann distribution

$$\frac{n^{1/2}}{n^{-1/2}} = e^{\frac{-h\gamma B_0}{2\pi kT}} \qquad [1]$$

where h is the Planck constant, k is the Boltzmann constant, T is temperature (in kelvins) and γ is the gyromagnetic ratio of the nucleus. A slightly higher amount of spins align along the B_0 field so that M points parallel to B_0 field, termed as a z-axis in the Cartesian coordinate system. In the xy-plane, the sum of vectors is zero. The spins precess at the Larmor frequency (ν_0 in Hz, ω in rad/s), ω_0, according to the Larmor equation

$$\omega_0 = \gamma B_0 \qquad [2]$$

Magnetisation along the z-axis cannot be directly detected. To generate nuclear magnetic resonance, an oscillating field has to be generated to perturb the magnetisation from its equilibrium. This oscillating field is accomplished by producing a perpendicular radio-frequency (rf) pulse using an rf transmitter coil (NMR takes place in the rf range, so the external fields are also known as rf fields). The pulse transiently tilts the magnetisation away from the equilibrium by inducing transitions between two spin states. The spin transitions occur at the Larmor frequency. The process of tilting the magnetisation from the z-axis to the xy-plane is called "excitation" whereupon the spins are said to have received a "90° pulse". An inverting "180° pulse" tilts the spins so that magnetisation is left along the –z axis. Following perturbation, the magnetisation starts to return towards its equilibrium state through relaxation (chapter 2.3.2). At the same time, the precessing magnetisation in the xy-plane induces current flow into the receiver coil, producing the measured signal, the free induction decay (FID).

2.2.2 Magnetic resonance imaging (MRI) and spectroscopy (MRS)

Biological (biomedical) research uses NMR for two purposes; firstly, to probe biochemical compounds of the sample (magnetic resonance spectroscopy, MRS) and secondly, to determine the spatial distribution of water (magnetic resonance imaging, MRI). The electronic shielding effect results in a small additional field that influences the effective field sensed by the nucleus. Consequently, nuclei in different "chemical environments" resonate at slightly different Larmor frequencies, a phenomenon termed as chemical shift. Because of this, individual chemical compounds can be identified and quantified by MRS. In MRI, the chemical shift information is usually of little interest. Instead, linear magnetic field gradients are employed to produce a deliberate distribution of resonance frequencies across the sample, leading to encoding of water according to the spatial location. A mathematical method called Fourier transformation (FT) is used to solve the frequencies present in the acquired signal. In the case of MRI, FT is applied to 2 dimensional MRI time domain, termed as k-space, along each axis to construct the image of water distribution in the sample.

State-of-the-art MRI and MRS share many technical details and can be performed in the same scanner. The time course of rf pulses and gradient switching is illustrated in Figure 1 for a classical spin-echo (SE) spin warp pulse sequence. Combination of the magnetic field gradients with frequency selective rf pulses allows the selection of a required slice from the sample. Following excitation, two further encoding methods are employed to fill the k-space. In one direction, a field gradient is employed during signal acquisition, making the NMR signal frequency encoded as described in the previous paragraph. The encoding of the signal along the other dimension is based on the fact that the frequency distribution of spins, caused by field gradient, inevitably also leads to a dispersion of their phases. The phase dispersion is dependent on the strength and length of the applied gradient. Phase encoding requires that the measurement be repeated with a number of different phase gradient strengths to provide

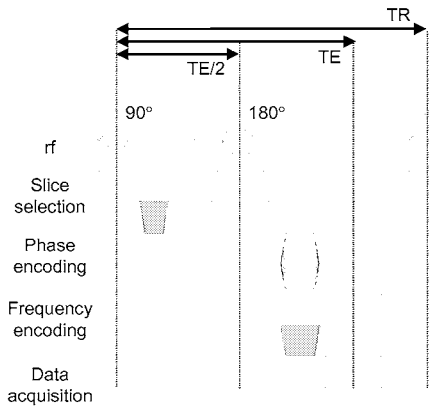

Fig. 1. Spin-echo (SE) imaging pulse sequence. Sequence combines selective rf pulses with gradients to achieve selection of required plane. Phase-encode gradient and read-out gradient encode the location of spins within the selected plane. Additional "rephasing" gradients (shaded) along slice select and read-out axis compensate for the phase dispersion caused by respective gradients. The 90° rf pulse excites the spins and the 180° pulse refocuses the spins generating an "echo" at echo time, TE. The sequence is repeated with different phase-encode gradient strenghts. The time between repeating excications is called repetition time, TR. Pulse sequence without 180° rf pulse is known as gradient echo (GRE) sequence. Alternatively, a pulse sequence with TE filled with repeated refocusing pulses is known as Carr-Purcell-Meiboom-Gill (CPMG) sequence.

enough phase data for FT, since the location of spins cannot be solved from a single experiment. In the SE method, a single line of k-space, corresponding to a single phase-encoding gradient strength, is acquired after each spin-echo pulse and the process is repeated until the whole k-space is filled. In modern MRI, a variety of pulse sequences with improved time resolution are also available. In these sequences, either several k-space lines are rapidly acquired following a single excitation, e.g. echo-planar imaging (EPI) and rapid acquisition with relaxation enhancement (RARE), or low flip angles and short TR are used, e.g. fast low-angle shot imaging (FLASH) [for further details, see e.g. (92)]. The pulse sequences used *in vivo* ^{1}H MRS share many common features with MRI sequences. In MRS, the gradients are used differently, however, since no frequency-encoding nor phase-encoding gradients are usually employed in order to retain chemical shift information. Instead, a series of rf pulses are applied in the presence of field gradients along each of the three axes to obtain volume selection within the sample.

2.3 Contrast in MRI and quantification of MRI parameters

It is obvious from Fig. 1 that there are several time dependent features in MRI, and in fact, the timing between the rf and gradient pulses can be utilised for contrast generation. This offers a possibility to widen the application of MRI beyond the imaging of the pure water content. A number of physical phenomena associated with molecular dynamics proceed during an MRI experiment and thus it is possible to reveal details of biological objects based on specific contrast mechanisms. Relaxation processes, communication of water molecules between the "free and semi-solid macromolecular pool", termed as magnetisation transfer, and molecular diffusion are the most important physical factors to be considered in the generation of MRI contrast. Substantial information exists about the contributions of these factors to MRI. However, it still remains a challenge to explicitly identify and quantify these effects, and in particular, in pathological conditions. In the following section, a review covering the basics of these physical mechanisms and methods for their quantification are described.

2.3.1 Spin density

Spin density, also known as proton density, is considered simply as the number of nuclei (protons) in the sample thus giving a robust estimate of tissue water content. As indicated above, the spin density is used as a MRI contrast, and indeed, a spin density-weighted image is easily obtained using a spin-echo sequence with long TR and short TE. Relaxation, diffusion and other effects, however, inevitably affect the observed spin density. Therefore spin density usually needs to be corrected for relaxation effects or calculated as the ratio between normal and abnormal tissue.

2.3.2 Relaxation

The signal behaviour determined by the relaxation processes is one the key MRI contrast used. The perturbed state of magnetisation is entropically intolerable and thus, magnetisation "relaxes" back to the thermal equilibrium with characteristic time coefficients. The relaxation processes involving exchange of thermal energy with spins and their environment, the lattice, are governed by T_1 relaxation, and the processes involving exchange of energy between the spins, leading to the loss of phase coherence in the xy-plane, are governed by T_2 relaxation. Consequently, T_1 is termed as spin-lattice relaxation and T_2 relaxation as spin-spin relaxation. The time-dependent changes in magnetisation governed by T_1 deal with the z and –z-axes, whereas the xy-plane is involved in T_2. Recovery of magnetisation to z-axis and decay of magnetisation in the xy-plane are described by exponential equations known as the Bloch equations (20)

$$\frac{dM_z}{dt} = \frac{M_0 - M_z}{T_1} \qquad [3a]$$

$$\frac{dM_{xy}}{dt} = -\frac{M_{xy}}{T_2} \qquad [3b]$$

where M_0 is the equilibrium magnetisation and M_z and M_{xy} are the magnetisation components along z-axis and in the xy-plane, respectively.

The relaxation occurring in the presence of rf field differs from the laboratory frame T_1 relaxation and is called $T_{1\rho}$ relaxation (120, 130, 212) or T_1 relaxation in the rotating frame. $T_{1\rho}$ relaxation time can be used to study T_1 at low magnetic field strengths. In $T_{1\rho}$ experiment, the spins are first tilted to the xy-plane and then effectively "locked" together with a long rf pulse of amplitude B_1. During the spin-lock, the distribution of frequencies is minimised. Instead, the spins relax along the rotating B_1 field through $T_{1\rho}$ relaxation.

The relaxation results from time-dependent fluctuations of magnetic or electronic fields generated by thermal motions of the diamagnetic or paramagnetic species. The fluctuating local magnetic fields are attributable to a number of factors including translational motion of molecules (diffusion), molecular rotations generating fields at the nucleus (rotation), chemical exchange, and fields generated by unpaired electrons (paramagnetic effect). In liquids,

rotational and translational processes can have major influences both on T_1 and T_2, while in more complex systems other mechanisms may also contribute significantly (70, 130). In the case of proton and other I=½ nuclei, the relaxation effects are mainly mediated through dipole-dipole interactions (23, 70).

The above mechanisms can cause relaxation only if there is a time-dependent interaction directly acting on the spins at an appropriate time scale, since only field fluctuations taking place at specific frequencies are effective at evoking relaxation. Frequency distribution can be described using spectral density functions of the form

$$J(\omega) \propto \frac{\tau}{1+\omega^2\tau^2} \qquad [4]$$

where τ is the correlation time, specific to the process involved and corresponds to the time required for a molecule to rotate one radian or the time between "jumps" in the orientation of its magnetic field (1, 70). In other words, the correlation time describes the time scale at which the given physical factors can influence spin behaviour. Dependence of relaxation times on different spectral densities can be described as (1, 21, 120, 153)

$$\frac{1}{T_1} \propto J^1(\omega_0) + J^2(2\omega_0) \qquad [5a]$$

$$\frac{1}{T_2} \propto J^0(0) + J^1(\omega_0) + J^2(2\omega_0) \qquad [5b]$$

$$\frac{1}{T_{1\rho}} \propto J^0(2\omega_1) + J^1(\omega_0) + J^2(2\omega_0) \qquad [5c]$$

where ω_0 is the Larmor frequency and ω_1 is frequency of the rotating frame B_1 field. It can be seen from the equations that while T_1 is sensitive to processes occurring close to the Larmor frequency (corresponding to τ of 10^{-7}-10^{-9} s), both T_2 and $T_{1\rho}$ are sensitive to contributions from processes occurring at much slower correlation times. Typical spin-lock fields used in $T_{1\rho}$ experiments are in kHz range corresponding to correlation times in the 10^{-2}-10^{-4} s scale. It can be also seen from the equations that T_2 relaxation is strongly affected by the mobility of molecules through contributions from "static" fields. The fast movement of molecules causes averaging of the different frequencies observed by the spins, thus making T_2 relaxation less efficient (so-called motional averaging). The contribution of the so-called lifetime broadening effect to both T_2 and $T_{1\rho}$ renders them shorter or equal to T_1 in all circumstances.

NMR relaxation *in vivo* is governed by interactions between the previously mentioned molecular diffusion and rotation, chemical exchange and paramagnetic and quadrupolar effects. The complex structure of cells and tissue as well as their chemical composition and endogenous chemical compounds results in a situation where water protons are exposed simultaneously to many factors which can influence the relaxation. In other words, tissues are magnetically inhomogeneous compared to simple liquid environment. Inhomogeneity and compartmentalisation exist both at the macroscopic (e.g. tissue and blood vessels) and

microscopic level (e.g. cellular organelles, membranes and protein surfaces). The water exchanges between the compartments with different time scales depending on restrictions, thus making the observed relaxation times differentially sensitive to these effects (54, 57, 70). Additionally dynamic processes such as CBF can contribute to the observed relaxation. In the following section, NMR relaxation is discussed separately for stroma, i.e. the body of the tissue, and parenchyma, i.e. the perfused tissue.

2.3.2.1 Relaxation in tissue

As stated above, tissues are inherently inhomogeneous from an NMR point of view and there are a number of either structural, biochemical or structural sources of static field variations. These field variations are one of the key sources of relaxation mechanisms. Much of the understanding from tissue NMR relaxation comes from the studies employing model phantoms such as gels and liquid and immobilised protein phantoms (7, 28, 91, 97, 132, 255, 265). The water relaxation has been explained using the N compartment model where different proton pools are in fast exchange (267) with each other (known as fast exchange two-state (FETS) or fast proton diffusion (FPD) model) (66, 71, 91). One of the pools represents free "bulk" water with τ of about 10^{-12} s. The relaxation times of bulk water are therefore practically independent of the used B_0 field, $T_1 = T_2 \sim 4$ s. Other pools represent protons with hindered mobility. In the simplest case, only one such pool, "bound water" pool, is assumed to exist. The correlation time of bound water is similar to protein protons, in the order of 10^{-3}-10^{-9} s. Alternatively, a distribution of bound pools, each with specific correlation time, can be assumed. It is assumed that spin diffusion and cross-relaxation relax the bound pool efficiently, so that the bound pool behaves as relaxation sink for the system. The important result of the model is that relaxation in tissue is dominated by intermolecular interactions between protons in macromolecules and water molecules even though only a small percentage of total water occupies the hydration water layer at any given time (23, 28, 70, 132).

One of the consistent observations from the model phantom (and also from *in vivo*) studies is the dispersion of T_1, i.e. increase of the spin-lattice relaxation rate as a function of the increasing Larmor frequency [for recent reviews on the subject see e.g. (28, 97, 131, 132)]. Knispel et al. suggested (130) that T_1 relaxation rate ($R_1 = 1/T_1$) in protein phantoms could be written as a sum of different contributing mechanisms with different correlation times as

$$R_{1,app} = R_{1,exch} + bR_{1,rot} + (1-b)R_{1,diff} \quad [6]$$

where $R_{1,app}$ is the observed relaxation rate, subscripts exch, rot and diff refer to exchange, rotational and diffusion contributions, respectively and b to bound water fraction (Fig. 2). Exchange processes can further be divided into 1) proton exchange (often also termed as chemical exchange) between water molecules and labile protons in –OH, -NH and -SH side chains on the protein surface and 2) exchange of magnetisation between protein and water molecules at specific buried binding sites (also termed as molecule exchange) (28, 54, 61, 97, 106, 130, 132, 145, 255, 260, 265). It should be noted that the two exchange processes differ

importantly from each other in the way the magnetisation is transferred between the protein and water molecule. In proton exchange, a water proton is covalently bound to the protein side chain thus replacing the labile proton. In contrast, in molecule exchange, the water molecule is hydrogen-bonded to protein at the binding sites and the exchange of magnetisation occurs through space via a dipole-dipole interaction known as cross-relaxation (28). The interaction requires that a water molecule is situated in close approximity to protein. The term molecule exchange reflects the fact that the residence time of an individual water molecule in the binding site is limited before a new molecule replaces it. Inside the protein, the magnetisation spreads through an efficient dipole-dipole interaction, often termed as spin diffusion. Similar mechanisms govern T_1 relaxation over a broad resonance frequency range from kHz ($T_{1\rho}$ experiments) to MHz (T_1 experiments) scale, yet the contribution of individual mechanisms will vary at different frequencies. Correlation times of the order of 10^{-6}, 10^{-8} and 10^{-10}s were proposed for the exchange, rotational and diffusion processes, respectively (130). It should be noted, however, that due to complexity of the system, calculation of correlation times *in vivo* may not be practical and the given times are only estimates.

The dispersion of relaxation times arises from either the "semi-solid" pool or from the interaction of magnetisation between the two pools, i.e. exchange. Brown et al. concluded in chemically immobilised protein phantoms that, dipolar-fields generated by the macromolecular rotations significantly contribute to the spin-lattice relaxation at low B_0 or in the rotating frame (27). An alternative explanation for the T_1 relaxation dispersion claims that chemical exchange between the bulk and semi-solid pools results in the phenomenon (7, 54, 61, 132, 229, 255, 265). It should be noted that the glutaraldehyde method commonly used for immobilisation, cross-links the proteins from -NH protons leading to the absence of exchangeable chemical groups (172) thus complicating the interpretation of data. Recent data suggests that $T_{1\rho}$ dispersion is mediated by proton exchange (59, 172) while dipolar

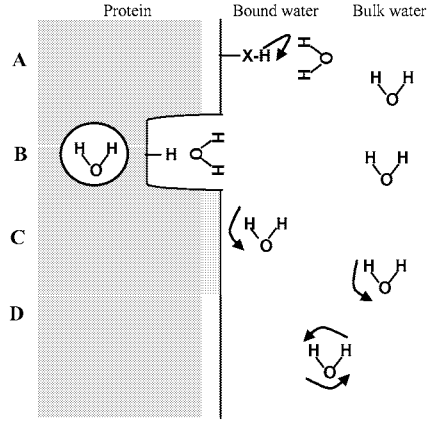

Fig. 2. Processes affecting water relaxation in protein solutions and tissue, where proteins act as relaxation sinks for the system. A) proton exchange through labile protons in side groups B) magnetisation exchange through water molecules in the binding sites and buried water sites. The magnetisation is exchanged through cross-relaxation. Slow protein tumbling creates dipolar fields that affect water relaxation C) rotation of bound water in the hydration layer and "diffusion exchange" on the surface of the protein. D) translational and rotational movement (diffusion) of bulk water. Water molecules are continuously exchanging between bulk and bound pools. Inside the protein, efficient spin diffusion relaxes the whole protein. Each process has its own correlation time thus affecting only specific relaxation pathways. Based on (27, 28, 70, 97, 130, 131, 145).

interactions in the molecule exchange pathway has been proposed to dominate T_1 dispersion (132). Furthermore, a consensus prevails claiming that magnetisation transfer *in vivo* operates mainly through a cross-relaxation pathway (80, 81, 106, 258).

Not surprisingly, very similar mechanisms are also operative for T_2 relaxation with a common relation proposed as

$$R_{2,app} = R_{2,int} + R_{2,exch} + R_{2,diff} \quad [7]$$

Thus, apart from the intrinsic or irreversible transverse relaxation governed by the mechanisms described previously, exchange and diffusion significantly contribute to R_2. The contribution of diffusion covers not only the translational effects, but also the susceptibility effects. This is due to the fact that during TE, water diffuses through magnetically different environments leading to additional dephasing. The commonly used SE methods can be differently sensitised to these physical factors (see chapter 2.3.2.3). It should be also noted that inhomogeneous B_0 field and susceptibility effects from interfaces cause phase dispersion that can affect T_2. While relaxation caused by the incoherent dephasing effects described previously cannot be reversed, the frequency differences caused by other effects are reversible by the spin-echo pulse sequence. Therefore effective T_2 relaxation time (T_2*) can be represented as a sum of two contributions:

$$R_2^* = R_2 + R_2' \quad [8]$$

where R_2 represents irreversible T_2 relaxation and R_2' represents reversible contribution caused by coherent dephasing effects from local field inhomogeneities and susceptibility differences. It is thus understandable that unlike T_1, T_2 decreases with increasing B_0 field because of the increased effects of the susceptibility differences.

Finally it can be noted, that $T_{1\rho}$ probes events taking place at much slower frequencies than T_1, thus being inherently similar to T_2. In fact, it has been shown that T_2 times obtained with Carr-Purcell-Meiboom-Gill pulse sequence with short delay between refocusing pulses (see chapter 2.3.2.3) and $T_{1\rho}$ at low B_1 fields give similar relaxation results (171, 191, 208). Interestingly, the dispersion of $T_{1\rho}$ as a function of B_1 field resembles that of T_1 (130), yet B_0 dispersion is similar to T_2 (62), showing that several mechanisms contribute to observed $T_{1\rho}$ relaxation times. In this instance, it should be emphasised, however, that $T_{1\rho}$ relaxation is significantly less sensitive to susceptibility effects provided that the B_1 field used is larger than local field inhomogeneities (201).

2.3.2.2 Relaxation in perfused tissue, parenchyma

In addition to previously presented interactions, constantly "dynamic" components, such as perfusion (or blood flow), may affect *in vivo* NMR relaxation. Flowing fluid within a MRI voxel results in an unavoidable loss of the excited spins. This influences parenchymal T_1 and can, in fact, be used for quantification of perfusion (see chapter 2.3.5). Flow may also affect *in vivo* T_2 measurements due to a TE–dependent signal loss.

From the functional point of view, it is interesting that transverse relaxation can be used to detect the blood oxygenation level dependent effects (BOLD) (25, 29, 184, 185, 231). BOLD contrast is generated by the local increase both in oxyhaemoglobin/deoxyhaemoglobin ratio and cerebral blood volume (CBV) leading to prolonged T_2* and T_2. The BOLD effect is mediated in blood water by exchange of water molecules between haemoglobin and plasma (75, 247) and diffusion of water molecules through field gradients (76, 231). BOLD is particularly intriguing for functional neuroimaging [for recent reviews on functional MRI applications, see e.g. (119, 164)]. Quantitative models describing the T_2* or T_2 BOLD effect in physiological equivalents have been published (44, 186, 247, 262). From the point of view of the present work, the intravascular single SE BOLD model (247) is of particular interest, since it has recently been employed for quantification of haemodynamic and metabolic adaptations to compromised haemodynamics (88, 125, 237, 247).

Table 1 collects together some of the physiological factors influencing *in vivo* T_1 and T_2 relaxation [for a systematic review of factors influencing *in vivo* relaxation see e.g. (23)]. $T_{1\rho}$ relaxation is not well known *in vivo*, yet it is likely to be influenced by similar factors (87, 90, 159, 172).

Table 1. Physiological factors influencing *in vivo* relaxation

	T_1	T2
Water content and free/bound water-ratio (protein mobility)	(23, 24, 65, 121-123, 147)	
Paramagnetic compounds	(40, 222)	(39, 99)
CBF/perfusion	(36, 52, 257)	
BOLD		(25, 184, 231)
Temperature	(23, 53, 121)	

2.3.2.3 Measurement of relaxation times

Solving the Bloch equations (eqs. [3a] and [3b]) yields respective equations for T_1 and T_2 relaxation

$$M(t) = M_0(1 - e^{-t/T_1}) \quad [9a]$$

$$M(t) = M_0 e^{-t/T_2} \quad [9b]$$

where M_0 is the steady-state spin density and t is time. By sampling magnetisation at different time points of the given NMR method, either T_1 or T_2 can be quantified.

An inversion recovery (IR) method is a common NMR means to determine T_1, in which magnetisation is inverted to –z-axis followed by sampling of the signal at different time points called inversion times (TI). This is accomplished by repeating the inversion pulses with a number of TIs or by repeatedly tilting a fraction of magnetisation to xy-plane and sampling the magnetisation during a single recovery curve. The latter sequence is known as the Look-Locker method. T_2 can be measured with a SE pulse sequence with different TEs and fitting

the observed decay curve to eq. [9b]. In this instance, it should be noted that there are several types of SE methods, each yielding T_2 with inherently different sensitivities to physical factors such as exchange and diffusion (5, 38). The two common SE methods used are single-echo (Hahn) spin-echo (Fig. 1) and Carr-Purcell-Meiboom-Gill (CPMG) multi-echo pulse sequences. In the former method, each echo is acquired after a single refocusing pulse, while the latter sequence consists of a train of refocusing pulses separated by a delay (τ_{CPMG}) and the echo is either collected after each refocusing pulse or after the entire train of pulses. Changing τ_{CPMG} strongly influences the exchange and/or diffusion contributions to T_2 (see chapter 4.7.10). At very short τ_{CPMG}, the CPMG refocusing pulse train approaches spin-lock (191, 208) conditions and, provided that the delay between the excitation and refocusing pulse train is also very short, T_2 approaches $T_{1\rho}$. Finally, it is worth stating that the previously mentioned reversible and irreversible contributions to T_2 (eq. [8]) can be separated by either using SE (T_2) and GRE (T_2*) methods separately (85), or directly with SE/GRE hybrid pulse sequences (6, 156). $T_{1\rho}$ can be quantified by altering the length of the spin-lock pulse (spin-lock time, SLT) and fitting the data to an exponential as in eq. [9b].

2.3.3 Magnetisation transfer (MT)

The concept of magnetisation transfer (MT) covers a group of MRI methods exploiting exchange of magnetisation between the bulk water and semi-solid macromolecular pools. MT is an expression of a previously mentioned exchange phenomenon (68, 267), in which the NMR properties of water molecules change due to interaction between two spin pools with different physico-chemical properties. The mechanism of magnetisation transfer mainly involves cross-relaxation through molecule exchange pathway *in vivo*, but evidence has been forwarded to show that proton exchange also contributes to MT in protein solutions (80, 81, 106, 258).

Wolff and Balaban first described *in vivo* MT in the late 80's (258). In an MT experiment, macromolecular protons are saturated with an off-resonance rf field called B_2, avoiding direct saturation of protons in the bulk water pool. This is possible since short T_2 [μseconds (106)] of macromolecular protons renders their line widths in the kHz range ($\Delta\nu_{½} \propto 1/T_2$). Due to exchange of magnetisation between the two pools, the B_2 pulse results in a signal loss of the bulk water thus creating the MT contrast. The contrast is generated by applying either a long "continuous wave" rf pulse (CW MT), or by short rf pulses (pulsed MT). MT contrast is pulse sequence dependent (106) due to the effects of incomplete saturation and the contribution of direct saturation of bulk water pool. One practical way to quantify MT is to calculate the ratio between saturated (M_{sat}) and steady-state magnetisation (M_0), known as magnetic transfer ratio (MTR) (81, 258)

$$MTR = 1 - \frac{M_{sat}}{M_0} \qquad [10]$$

A thorough quantification of MT variables requires acquisition of M_{sat} values at multiple offsets [the Z spectrum (80)], and B_2 fields. Using a two-pool model of exchange, one can then determine the relaxation characteristics of individual spin pools as well as exchange rates between the pools (105, 106).

2.3.4 Diffusion

Diffusion is an expression of thermal "Brownian" motion of molecules. During an observation period, molecules move randomly with a mean squared displacement $\langle r^2 \rangle$ according to the Einstein equation

$$\left\langle r^2 \right\rangle = 6Dt \qquad [11]$$

where D is the inherent molecular diffusion coefficient. This relation applies to isotropic diffusion, i.e. to the condition where diffusion is equal along all directions of space. Translation of molecules in a gradient field generates random phase dispersion of spins (93) and leads to an exponential decay of magnetisation. NMR experiment can be sensitised for diffusion by placing a pair of pulsed field gradients ("diffusion gradients") into a SE pulse sequence (219, 225), usually symmetrically with respect to the refocusing pulse. The first diffusion gradient "labels" the spins and the latter gradient "refocuses" the spins not undergoing diffusion during the time between the gradients.

Diffusion coefficient and the strength of diffusion sensitising gradients govern the rate of the magnetisation decay

$$M = M_0 e^{-bD} \qquad [12]$$

The effect of diffusion sensitising gradients is described by "b-value" which in the case of a pair of rectangular diffusion gradients has the form

$$b = \gamma^2 \delta^2 G^2 (\Delta - \delta/3) \qquad [13]$$

where G and δ are the amplitude and duration of the diffusion gradient, respectively and, Δ is the time between diffusion gradients.

Diffusion *in vivo* is seldom isotropic, but becomes orientation dependent, i.e. anisotropic. This is understandable, since membranes and cellular structures create inherent restrictions for molecular diffusion. In addition, exchange of water across membranes leads to a situation where water may experience different microenvironments with different inherent diffusion coefficients during the data acquisition. For this reason, the diffusion coefficient determined *in vivo* is termed as an "apparent diffusion coefficient", ADC (138, 139). Furthermore, because of anisotropy, a scalar diffusion coefficient is not adequate to describe *in vivo* diffusion accurately (138). Diffusive transport, however, can be characterised by a second-rank tensor of nine diffusion coefficients, **D**, that also takes into account the interaction between diffusion gradients (14) [for a more detailed description of diffusion tensor and its applications, see recent review by Le Bihan (140)].

$$\mathbf{D} = \begin{bmatrix} D_{xx} & D_{xy} & D_{xz} \\ D_{yx} & D_{yy} & D_{yz} \\ D_{zx} & D_{zy} & D_{zz} \end{bmatrix} \quad [14]$$

The measurement of full diffusion tensor provides unique information concerning anatomical details of the tissue including fibre orientations and connectivity in the brain (15, 140, 165). The trace of the diffusion tensor,

$$\mathrm{Trace}\mathbf{D} = D_{xx} + D_{yy} + D_{zz} \quad [15]$$

is an orientation-independent quantity to be used to describe average diffusion without measuring the full tensor (49, 167, 244, 259)

$$D_{av} = \tfrac{1}{3}\mathrm{Trace}\mathbf{D} \quad [16]$$

2.3.5 Imaging of haemodynamics

MR methods known as "perfusion imaging" allow for quantitative imaging of haemodynamic variables including CBV, CBF and mean transit time (MTT). The most widely used method for perfusion imaging involves the use of paramagnetic MR contrast agent. The technique, known as dynamic susceptibility contrast MRI, (DSC-MRI, "bolus tracking") is now commonly used to image haemodynamics for physiology and pathology purposes (36, 99, 227, 269). More recently a technique based on "magnetic" labelling of arterial blood by rf field was developed (52, 257). These techniques are known as "arterial spin labelling" (ASL) methods (36, 52, 127, 257).

In DSC-MRI, an intravascularly distributed paramagnetic contrast agent, such as Gadolinium (III) - diethyltriaminepentaacetic acid (Gd-DTPA), is rapidly injected into a peripheral vein. Once the "bolus" of the contrast agent reaches the region-of-interest, a short blood relaxation time due to the paramagnetic label leads to a decline in MRI signal intensity acquired either by a SE or GRE method. A series of perfusion variables including bolus arrival time and peak intensity can be directly derived from the signal time course, and importantly, the kinetics of MR signal behaviour makes it possible to determine absolute CBV, CBF and MTT (see e.g. (36, 268, 269) for further details in modelling and limitations of methodology). Blood pool contrast agents with long (>hour) plasma half-lives such as dextran-coated iron oxide particles have recently been introduced in animal studies of CBV (98, 205).

In ASL methods, the labelling of blood is accomplished by either saturating or inverting the spins flowing into the area of interest using rf pulses. The labelled blood water then exchanges at the capillary level with extravascular water leading to reduction in the MR signal intensity (52, 257). A subtraction of labelled image from non-labelled control image produces a perfusion image with signal intensity proportional to CBF. Both continuous and pulsed rf labelling schemes have been published (36). Continuous ASL (CASL) methods use a long low-power rf pulse at the level of the neck to label the in-flowing arterial blood (52, 257), while pulsed ASL (PASL) methods use short labelling pulses localised close to the volume of

interest (60, 127, 134). ASL methods can produce quantitative CBF maps with high spatial resolution. Indeed, CBF values reported by ASL methods agree with those obtained by other modalities (36). As far as the use of ASL methods for cerebrovascular disease are concerned, prolonged transit time, leading to reduced labelling due to T_1 relaxation of the blood, may hamper quantification of CBF.

To complete the repertoire of MRI methods for imaging of cerebral "haemodynamics", the anatomy of the vasculature can be imaged using magnetic resonance angiography (MRA) (82) methods. MRA methods resembling diffusion imaging also allow for the estimation of perfusion based on phase dispersions caused by the blood flow (139).

2.4 MRI of compromised cerebral haemodynamics

It is clear from the above data that multimodal MRI methods are inherently suited for the assessment of brain suffering from haemodynamic crisis. Indeed, very soon after the MRI scanners became available in early 80's, the technology was applied to both experimental and clinical ischaemia (31, 217). Substantial research efforts both in experimental and clinical settings have provided the basis for the central role of MRI in pathophysiology studies of acute stroke (107), development of new treatment strategies and drugs (204), and patient management (12, 181).

2.4.1 Cerebral ischaemia

The medical term "ischaemia" is used to depict a state of severely compromised haemodynamics thus covering a spectrum of haemodynamic conditions. Brain ischaemia syndromes are divided into two groups according to the haemodynamic state as follows; firstly, global ischaemia and secondly, focal ischaemia (235, 254). Global brain ischaemia results from "complete" cessation of blood supply to the brain and develops for instance after cardiac arrest, severe cardiac failure or strangulation. Global ischaemia can be either complete (no flow) or incomplete (some residual perfusion). In the latter condition, residual flow prevails, but below the level needed to maintain oxygen and glucose supply for mitochondrial energy metabolism. Focal ischaemia (this condition is the well-known ischaemic stroke) is a consequence of locally compromised flow due to arterial blood clot or atherosclerotic occlusion. It should be noted that brain has a special vascular system called the Circulus of Willis forming an efficient communication between the main feeding arteries, i.e. the carotids and vertebrales, which can supply blood to the ischaemic volume through the "collateral" vessels. From a haemodynamic point of view it is thus obvious that the perfusion conditions in global and focal brain ischaemia greatly differ. It would be anticipated that this difference would have an impact on the pathophysiology of the two syndromes as well as on the development of MRI contrasts in the early minutes of the insult.

Cerebral haemodynamics possesses a number of compensatory mechanisms to resist the decline of CBF at reduced cerebral (central) perfusion pressure (CPP). Reduction of CPP below the level of autoregulation (about 70 mmHg) is compensated by an increase in CBV. A

continuing decrease in CPP leads to an increase in the oxygen extraction ratio (OER) maximally by 2.5-fold (198, 254). Therefore despite the low CPP, substrates are supplied for oxidative phosphorylation. At CBF values of 35-55 ml/100g/min, inhibition of protein synthesis develops (160, 261), and weakening of synaptic function to the evoked potential has been observed (77, 111). Either a global or focal subtle drop of CBF below a level of 20 ml/100g/min, results in a rapid decline in adenosine triphosphate (ATP), acidification, build-up of lactate and cessation of evoked potentials and electroencephalographic (EEG) activity (9, 104, 111). Ischaemia at this CBF level is still considered to be reversible provided an early reperfusion occurs. A drop of CBF to 10-15 ml/100g/min leads to a collapse of ionic homeostasis expressed as anoxic depolarisation, which is associated with a shift of ions across the cell membrane. The movement of ions elevates intracellular osmolality causing a shift of water into the cell interior and a reduction of the extracellular space (ECS) (101, 115, 183). The concept of critical CBF thresholds for cerebral ischaemia bears clinical and therapeutic implications (111, 182). However, it should be noted that CBF thresholds have a significant temporal component and the "ischaemic energy failure" tends to develop at higher CBF levels during the course of compromised haemodynamics (111).

The focal decline of CBF below the level expressing the energy failure produces an ischaemic "core". The core represents a tissue volume that becomes subjected to permanent damage if the arterial occlusion is not "reversed" spontaneously or by a treatment procedure. A volume of tissue surrounding the core may have an insufficient blood supply, which is above the level of ischaemic energy failure. This volume is referred to as "penumbra". The penumbra shows decreased electrical activity, yet persistent cellular integrity for a substantial period of time (9, 77, 111, 209). The penumbra is thought to represent tissue at risk of becoming damaged, yet potentially salvageable at the time of diagnosis (12, 111). A large body of data both from experimental and clinical settings supports this concept (94, 108, 109, 111, 203, 223).

One of the most immediate effects of genuine ischaemia is a rapid exhaustion of oxygen levels. Oxygen is used within 20 seconds of ischaemia (158, 174) while glucose is still available for anaerobic metabolism. As a consequence, cells start to produce ATP through anaerobic glycolysis leading to accumulation of lactate, which leads to acidosis (149, 216). After 2-3 minutes, glucose is used up and ATP and phosphocreatine (PCr) levels collapse (133, 141, 216). The absence of chemical energy terminates the energy-requiring processes including membrane ion pumps. This leads to a massive shift of ions across the plasma membrane and cell swelling (100-102). These events are completed within 5-7 minutes of ischaemia. One of the most destructive intracellular signals caused by ischaemia is the rise in intracellular calcium levels. The elevated calcium levels promote proteolysis and lipolysis, resulting in breakdown of vital components of the cell metabolic machinery such as enzymes, and structural components such as cytoskeleton and membranes in nucleus and cytoplasm (26, 118, 149, 195). In focal or incomplete ischaemia, conditions favouring net water accumulation

prevail during the insult (18, 41, 122, 133, 170, 251, 264), but the most excessive water shift into the tissue is known to require reperfusion (10, 18, 41). It should be pointed out that during complete ischaemia or following cardiac arrest, minimal water accumulation prevails (41).

Following short ischaemic periods, CBF may become reinstated. The robust alterations in metabolism and ionic and neurotransmitter homeostases lead to an overshoot in CBF as well as in CBV (112, 135, 218, 232-234). This phenomenon is termed as "luxury perfusion" and was originally described in humans during the 1960's (137). The hyperperfusion phase may be followed by a period of hypoperfusion (135, 218, 234). It has been reported that the oxidative and intermediate metabolism recover with slower kinetics than the haemodynamics, but protein synthesis is depressed much longer than other metabolic processes in the post-ischaemic brain (4, 114, 149, 200, 218). Electrical activity may resume after the restoration of energetic and ionic homeostasis (104, 176, 233). It should be noted that the recovery might look apparently complete, yet a "secondary" collapse of cellular energetics may develop subsequently (154, 245).

2.4.2 NMR methods in experimental ischaemia models

The interest of neuroscientists, neurologists and radiologists towards *in vivo* NMR methods in conjunction with cerebrovascular disorders arose decades ago. Both ^{1}H and ^{31}P NMR spectroscopy have been applied to the studies of experimental brain ischaemia revealing that the energetics, intracellular pH (pH_i) and build-up of lactate can be monitored in the different phases of the insult (2, 8, 42, 73, 230, 252). However, due to the poor spatial resolution of NMR spectroscopy methods, it has become obvious that these techniques are valuable only for certain purposes.

First *in vivo* MRI findings from experimental ischaemia models were reported in the early 1980's showing prolongation of T_2 and T_1 relaxation times after a few hours of ischaemia (22, 30, 110, 121-123, 157). It was demonstrated that prolonged relaxation times correlated with the water content *in vivo* (65, 110, 121-123, 147, 177). Water accumulation is an expression of irreversible ischaemia in the focally ischaemic brain or often also in the tissue with restored CBF after a global insult. Therefore, tissue with signs of long T_1 and T_2 relaxation times in MRI most often represents developing or mature infarction. In line with this idea, increased spin density was shown to be associated with T_2 contrast one day after induction of focal ischaemia (128, 190). Interestingly, a recent study has indicated that destructive processes, such as proteolysis, may also contribute to the prolongation of T_1 relaxation time during the evolution of ischaemia (64).

One clear breakthrough in the field of MRI took place in 1990 when Moseley et al. reported that the water diffusion coefficient became reduced within the first hour of ischaemia (168) and at this time point T_2 showed no abnormalities. They showed that the cerebral energy state, as revealed by ^{31}P NMR spectroscopy, was collapsed in the tissue with reduced diffusion. Moseley et al. suggested that ischaemic energy failure was one of the primary factors causing reduced water diffusion. Indeed, Busza et al. reported that the CBF level

leading to a decline in water diffusion was about 20 ml/100g/min, thus being virtually the same as for the collapse in ATP (33). Subsequently, diffusion MRI has rapidly gained acceptance both in experimental and clinical settings (12, 181).

After the pioneering work of Moseley et al., it soon became apparent that the decline of water diffusion is a robust response in the brain to a variety of noxious insults, such as injection of N-methyl-D-aspartate (NMDA) (19) and spreading depression (32, 45, 223). These observations are interesting in the search of the pathophysiological events leading to reduced diffusion. A two-compartment model comprising of extracellular and intracellular compartments has been employed in efforts to understand water diffusion *in vivo* (19, 196, 220). According to the model, diffusion in the extracellular space (ECS) is almost free, being restricted only by cell membranes, whereas in the intracellular space high viscosity and cell organelles substantially restrict molecular Brownian motion. In ischaemia, the shift of water from ECS to the cell interior and a reduction of ECS are considered to account for the decline in water diffusion (17, 19, 161, 163, 169, 239, 243, 244). The good match between diffusion changes (43, 46, 47, 50, 103, 116, 117, 197, 246) and the ionic changes and ECS shrinkage (101, 102, 183) support this hypothesis. Careful analyses of temporal relations have suggested, however, that substantial changes in diffusion MRI may occur prior to anoxic depolarisation, indicating that other mechanisms are also likely to contribute to the ischaemic diffusion change (103, 116, 117, 150). Diffusion MRS using intracellular and extracellular markers showed a similar drop in diffusivity in intra- and extracellular compartments in global ischaemia (58). In addition, the similar behaviour of diffusion of water and intracellular metabolites supports the hypothesis that a true change in intracellular diffusivity may be the key factor underlying the ischaemic diffusion drop (55, 96, 242, 256). Possible mechanisms explaining the reduced intracellular diffusivity include increased intracellular viscosity and cessation of energy dependent intracellular "streaming" (55, 58). Furthermore, it has been shown that a Ca^{2+}-dependent intracellular mechanism may significantly contribute to diffusion changes in the energetically compromised brain tissue (96).

The magnitude of ischaemia-induced reduction in diffusion coefficient is typically 15-30% over the first minutes of the ischaemic insult (43, 46, 227). A 5% drop of water ADC has been observed prior to a large collapse of diffusion, potentially reflecting a drop in CBV or intravascular susceptibility changes (47, 56). During the evolution of ischaemia, there is a maximal 40-50% decrease in ADC (35, 43, 109). It has been proposed that in focal ischaemia, diffusion MRI may potentially be used to differentiate core (diffusion < 80% of control) from penumbra (109, 188).

In permanent focal ischaemia, diffusion remains low for several days until it begins to increase 24-48 h after the onset of ischaemia. This phenomenon is called "pseudo-normalisation" and it is associated with clearance of damaged cells and their replacement with astroglia (12). In a more chronic state of ischaemia, diffusion is elevated. By combining diffusion and T_2 MRI, one can separate acute from subacute and chronic ischaemia, and in

fact, models based on the quantitative MRI of these two contrasts have been proposed for use to identify the different stages of ischaemic damage.

The data above clearly show that diffusion MRI is of great value in imaging of acute and subacute ischaemia. Substantial efforts have been placed to exploit diffusion MRI as a predictive index of tissue outcome. Unfortunately, many confounding factors have been reported for interpretation of diffusion MRI. One of these factors is that diffusion may temporarily recover upon restoration of flow even when an infarct develops over the subsequent days (35, 43, 90, 113, 142-144, 161, 162). Consequently, it appears that the outcome predictive value of a single time point diffusion MRI is low (197).

DSC-MRI probes directly the haemodynamics. Therefore it is capable of highlighting brain regions suffering from reduced perfusion "hypoperfusion" or ischaemia through delayed bolus arrival/washout, reduced CBV, prolonged MTT or even a complete absence of perfusion (36, 227). It should be noted, however, that even if the information obtained from DSC-MRI is of great value in the assessment of acute stroke patients, it is only "a mechanical" measure of perfusion, and does not provide any direct insight into the tissue viability. A recent work combining DSC and diffusion MRI advanced the predictive value of each of the methods by introducing the concept "perfusion/diffusion mismatch" (12, 13, 248, 268, 269). It was shown that in the cases where perfusion MRI showed a much larger volume of abnormality than diffusion MRI (the condition termed as perfusion/diffusion mismatch, suggested to represent "penumbra"), the final stroke volume approached that shown by DSC-MRI, unless the vascular occlusion was reversed. In contrast, in cases where initially similar volumes of damage were revealed by the two methods, the stroke volume did not grow.

As reviewed above T_1, T_2 and diffusion MRI using altered physical properties of endogenous water together with DSC-MRI with exogenous contrast agents can reveal both tissue and haemodynamic changes in acute and subacute cerebral ischaemia. Significant progress has been made in the further exploitation of endogenous contrast mechanisms in (hyper)acute ischaemia using relaxation –based contrast. The studies using T_2* or T_2 MRI challenged the conventional concept of transverse relaxation as being a sign of irreversible ischaemia. It was reported that during hypoxia, in the early minutes of global ischaemia and in focal ischaemia even for substantial periods of time, there is a reduction in transverse relaxation times instead of the well-known increase (35, 48, 85, 89, 125, 155, 202, 236). Shortening of transverse relaxation time was associated with reduced blood oxygen saturation level and indeed, in a focal ischaemia model it has been shown to require collateral flow (202). Gröhn et al. recently showed that the negative BOLD effect was expressed at a CBF level of below 60% of normal with maximal negative BOLD occurring at CBF of 30 ml/100g/min, a flow value below which the cerebral metabolic rate of oxygen ($CMRO_2$) is known to become inhibited (88). The intravascular quantitative SE BOLD model by van Zijl et al (247) was able to explain the entire parenchymal T_2 decline in acute flow compromise to be due to BOLD. This is interesting, since T_2 MRI can be expected to reveal a mismatch between the oxygen

delivery and consumption to the brain and on the other hand, negative BOLD would be possible only through active oxygen extraction by the tissue (86). Lin et al. have used BOLD MRI in clinical settings attempting to quantify OER and $CMRO_2$ in stroke patients (146).

Another "surprising" observation has been that there is an early T_1 prolongation in the ischaemic brain, well before net water gain (35). In some regards, the T_1 prolongation would be expected, since CBF as such influences parenchymal T_1. On the other hand, it has been speculated that a part of the acutely increased cerebral T_1 may be due to other factors such as exhaustion of tissue oxygen or microenvironmental physico-chemical changes (35, 155).

Very recently it was reported that $T_{1\rho}$ or dispersion of $T_{1\rho}$ are sensitive MRI markers of acute ischaemia (87, 90). $T_{1\rho}$ increases up to 30 % of control were detected within the first hours of focal ischaemia. Interestingly, in a rat model of transient focal ischaemia, $T_{1\rho}$ when quantified in the early minutes of reperfusion provided a high predictive value of the degree of neuronal loss that was determined 24 hours after the insult (87). The CBF threshold for acute $T_{1\rho}$ contrast was shown to be about 20 ml/100g/min, thus being very similar to that of energy failure and generation of diffusion contrast (87). The pathophysiological factors causing the acute $T_{1\rho}$ contrast are evidently of substantial scientific interest.

2.4.3 MRI in the assessment of tissue status

Considerable efforts have been placed to derive predictive models of tissue outcome from single time point MRI data, a situation most closely resembling clinical work. It has become clear that no single MRI parameter is able to predict the outcome of tissue, and thus a multimodal MRI would be needed. As indicated above, perfusion/diffusion mismatch is currently a very appealing way of revealing reversible ischaemia in human stroke patients (269), and obviously, one can combine T_2 relaxation data into it to complement this model of tissue status. Welch et al. introduced the concept of "tissue signatures" for diffusion and T_2 MRI (253). The model of Welch et al. was intended to assign developing and consolidated infarct with an aim of giving the point-of-no-return for the clinician. Many groups have recently revised the model (35, 37, 67, 89, 227). The recent revisions are aimed at separation of irreversible and reversible ischaemia, for instance in the revised model by Gröhn et al. (86), the negative BOLD effect is used as a marker of reversibility.

2.4.4 MRI in the studies of human acute stroke

A trend toward an active treatment of patients suffering from acute brain insults including stroke is imminent (12, 148). Currently recombinant tissue plasminogen activator (rt-PA) (83) is in use for stroke treatment with several other drugs in clinical trials. Since the first clinical applications of MRI for stroke (206, 217), it has become clear that MRI possesses a better capability to delineate ischaemic tissue from non-ischaemic tissue as compared to the computed tomography (CT). As indicated earlier, the diffusion MRI paper by Moseley et al. (168) certainly multiplied the clinical interest towards the use of MR methods as such for the

diagnosis of acute cerebrovascular conditions in clinical settings (168, 250) and since then MRI has become the method of choice for acute stroke diagnosis (181).

It has been interesting to note that a number of MRI observations emerging from experimental stroke models have been found to be applicable in stroke patients. These include the time courses of T_2 and diffusion MRI contrasts during the evolution of ischaemia, normalisation of diffusion after thrombolytic treatment followed by a secondary decline in the areas subjected to damage and the presence of negative BOLD in the early hours of stroke at 1.5 T (12, 13, 16, 126). One of the main differences has been the time course of contrast development, for instance reduced diffusion may be detectable for 4-10 days after the onset of early symptoms (136, 210, 238) and a perfusion defect without any reduced diffusion may be present for days (11, 248). The differences may reflect haemodynamic characteristics of species.

A state-of-the-art protocol for imaging of acute cerebrovascular condition would include diffusion, perfusion and T_2 weighted MRI with a possible extension of MRA for detection of vascular occlusion or T_2* MRI for estimation of haemorrhage (12, 13, 181). In particular, diffusion/perfusion mismatch has proved to be a working concept in clinical settings (12, 16, 181, 221). It should be noted that clinical radiologists usually work with MR images acquired with weighting to a given contrast rather than those displaying absolute values. The convention of using weighted images certainly places limits for the possibility of detecting 2-10% relaxation changes and also it requires high B_0 and B_1 homogeneity from the MR scanner.

3 AIMS OF THE STUDY

It is firmly established that MRI rapidly and reliably identifies the tissue suffering from an ischaemic insult. Recent experimental studies have suggested that a substantial body of novel pathophysiologic information would become available through absolute quantification of T_1, T_2, or $T_{1\rho}$ MRI in hyperacute cerebral ischaemia and that this information may be useful in the assessment of tissue viability (35, 87, 89). The aim of the present work was to study the pattern of these MR relaxation changes in the very first minutes of ischaemia in various animal models and to explore the contribution of pathophysiologic factors to the MRI contrast generation. A special focus was placed on the effects of haemodynamic factors, macroscopic and microscopic susceptibility, tissue acidification and water accumulation. The goal was to distinguish between the intravascular and tissue effects on the MR relaxations and thus, to assign the contrast generation mechanisms to a given pathophysiologic factor associated with hyperacute stroke.

The specific aims in these studies were as follows:

1) to estimate the contribution of CBF to parenchymal T_1 relaxation time in the rat global and focal ischaemia models. In the latter model, the value of T_1 MRI in the prediction of tissue outcome was also investigated.

2) to explore $T_{1\rho}$ relaxation in acute ischaemia and to identify the contributions of physico-chemical alterations in the intravascular and tissue compartments. The experiments were designed to address the contribution of loss of ionic homeostasis to the changes in $T_{1\rho}$ relaxation time induced by ischaemia, as well as to study the effects of intracellular pH, BOLD and haemodynamic factors, and tissue oxygen tension.

3) to apply the intravascular SE BOLD model (247) for the assessment of haemodynamic and metabolic recovery after a brief cerebral ischaemic insult.

4 MATERIALS AND METHODS

4.1 Preface

In the following, the methods used in the current studies are briefly summarised. For further details, see individual publications (**I-IV**).

4.2 Animals

Male Wistar rats (National Laboratory Animal Centre, University of Kuopio) weighting 250-350 g were used. Animals were fed *ad libitum* (**I, II, IV**) or fasted overnight (**III**). The National Laboratory Animal Centre at the University of Kuopio approved all animal experiments.

4.3 Anaesthesia

For T_1 experiments, MRI animals were initially anaesthetised with 4.0 % halothane in 70%/30% N_2O/O_2 and maintained with 1.0-1.5 % halothane for surgery after which anaesthesia was switched to α-chloralose (slow bolus of 80 mg/kg i.v., 20 mg/kg hourly) (**I**). In $T_{1\rho}$ experiments, either 0.7-1.2 % halothane in 70/30 N_2O/O_2 (global ischaemia experiments induced by cardiac arrest) or 1.2-1.5 g/kg, i.p. urethane (all electrophysiology and hypoxia or hypercapnia experiments) was used (**II, III**). In T_2 BOLD MRI (**IV**), the animals were anaesthetised with halothane for electrocoagulation of vertebral arteries and re-anaesthetised three days later with urethane for following surgery and MRI and CBF determination.

4.4 Physiological monitoring

Blood gases and pH were analysed from blood samples obtained through a femoral artery line [ABL-5, Radiometer Inc., Copenhagen, Denmark (**I, III**) or i-STAT, i-STAT Co., East Windsor, NJ, USA (**II, IV**)] during MRI experiments at the time points indicated in the individual articles. Blood glucose was assayed [One Touch Basic, Lifescan Inc., Milpitas, CA, USA (**III**), Precision Q.I.D., Medisense, Inc, Bedford, MA, USA (**IV**)]. Mean arterial blood pressure (MABP, CardioCap II, Datex, Helsinki, Finland) via femoral arterial cannulae and body temperature were monitored on-line during surgery and MRI (**I-IV**), and core temperature was maintained close to 37 °C by circulating warm water in a heating element (**I-IV**) or by blowing warm air through the magnet bore (**I**).

4.5 Animal models

Transient middle cerebral artery occlusion (MCAO) was produced using the intraluminal thread model of Longa (152) (**I**). Briefly, a nylon thread (diameter 0.22 mm) was inserted into the right common carotid artery (CCA) until the opening of the MCA became blocked. Rats were transferred into the magnet immediately after the occlusion. The thread was retracted after 20 or 90 minutes of occlusion while the rat was inside the magnet. In sham-operated

animals, the thread was inserted only to the opening of the internal carotid artery leaving the MCA flow intact.

A four-vessel model proposed by Pulsinelli et al. (199) was modified for graded CCAs occlusion and global ischaemia studies (**IV**) as previously described (88). Briefly, both vertebral arteries were occluded by electrocoagulation three days prior to CCA occlusion. CCAs were exposed and surrounded with silicon-coated snares joined to a controllable screw device as previously described (88). The device allowed either for graded or complete occlusion and release of CCAs while the animal was inside the magnet. Two animal groups with either a 15-minute graded CCA occlusion followed by complete ischaemia or complete ischaemia of 7 minutes, both with subsequent reperfusion, were studied. In the animals exposed to graded CCA occlusion without drop in water diffusion coefficient, a complete occlusion of CCAs for 15 minutes was induced after a recovery period of 30 minutes.

For hypoxic hypoxia, hyperoxia or hypercapnia experiments, the rats were mechanically ventilated (Harvard Instruments Small Animal Ventilator, Boston, MA, U.S.A.) (**II**). The inspired oxygen level was altered to either 100% or 10% to induce hyperoxia or hypoxic hypoxia, respectively. Hypercapnia was produced by adding 10-40% CO_2 to inhaled gas mixture through the ventilator.

Global ischaemia was induced by cardiac arrest with a bolus injection of saturated KCl i.v. during MR data acquisition (**I, II, III**). Cardiac arrest was verified from the collapse of blood pressure (pressure drop below 15 mmHg) and visually observed cessation of breathing. Pre-ischaemic hyper- or hypoglycaemia (**III**) was induced by giving either 2.5 ml of 50% glucose solution or 3 IU/kg of human insulin (Orion Pharmaceuticals Inc, Espoo, Finland) intraperitoneally, respectively, 30 minutes prior to the global ischaemia experiments.

4.6 Electrophysiology

4.6.1 Tissue oxygen tension (PtO_2)

Tissue oxygen tension (PtO_2) was quantified using custom-made carbon-fibre electrodes (**II**). Two carbon-fibre electrodes coated with glass (diameter of 30 μm) were inserted into both sides of cortex 1.5 mm caudal to bregma and 3 mm lateral from the midline to a depth of 500 μm, with reference electrodes inserted subcutaneously in the flank. The oxygen-sensitive electrodes were polarised with a reduction voltage of -0.7 V.

4.6.2 DC potential

DC potentials were recorded using a platinum/iridium electrode inserted into the somatosensory cortex 1 mm caudal to bregma and 3 mm lateral from midline to left side of the brain (**III**). Ag/AgCl reference electrodes were inserted subcutaneously in the flank. Measurements were continued for the duration of MRI experiment. Electrophysiological measurements and MRI were synchronised based on MRI artifacts present on the DC traces. Prior to the analysis of DC traces, a median filter was used to reduce the artifacts.

4.6.3 Cerebral blood flow

CBF was quantified (**IV**) using the hydrogen clearance method (42, 88, 263). Briefly, two 1 mm platinum/iridium electrodes were inserted 1 - 1.3 mm into both sides of cortex 1.5 mm caudal to bregma and 3 mm lateral from midline. Ag/AgCl reference electrodes were inserted subcutaneously in the flank. A hydrogen clearance curve was recorded following the inhalation of $H_2/N_2/O_2$ 10/65/25 (%/%/%) gas mixture and analysed using the initial slope approach (189).

4.7 Nuclear magnetic resonance methods

4.7.1 Hardware

Magnetic resonance data were acquired using a 4.7 T horizontal magnet (Magnex Scientific Ltd, Abington, UK) interfaced to an s.mi.s. console (Surrey Medical Imaging Systems Ltd, Guildford, UK, **I**, **III**, **IV**) or Varian ^{UNITY}*INOVA* console (Varian Inc, Palo Alto, California, USA, **II**, **IV**) and 9.4 T vertical magnet (Oxford Instruments, Oxford, UK) interfaced to an s.m.i.s. console (**I**). Both magnets were equipped with actively shielded field gradients (Magnex). Home-build surface coils, tuned to ^{1}H frequencies of 200 and 400 MHz, were used for both transmitting and receiving. A linear birdcage/surface coil transmitter/receiver pair was used for MT measurements (**III**). A $^{1}H/^{31}P$ surface coil was used for hypercapnia experiments (**II**). Cerebral T_1 was quantified at 1.5 T (Siemens Vision+, Siemens AG, Erlangen, Germany) using a body resonator for signal transmission and a surface coil for signal detection (**I**).

4.7.2 The apparent diffusion coefficient

The trace of the diffusion tensor (D_{av}) was quantified using a single SE sequence with four or eight bipolar gradients along each axis (167). The sequence was either an imaging sequence with a non-selective adiabatic BIR-4 (74) refocusing pulse (**I, IV**) or a line-scan sequence (116) with selective sinc pulses (**II, III**). ADC with diffusion gradient along x-axis was measured using a modified driven-equilibrium Fourier transform (DEFT) sequence (**I**) with a pair of diffusion-sensitising gradients around the 180° refocusing RF pulse in front of a FLASH imaging scheme (228).

4.7.3 T_1, $T_{1\rho}$ and T_2 relaxation times, spin density and MTR

An IR fast spin-echo sequence was used to determine T_1 at 1.5 T. At 4.7 and 9.4 T, T_1 was quantified using a non-selective adiabatic inversion pulse followed by a crusher gradient in front of either a FLASH imaging scheme (**I**) or a line-scan sequence (**II**). In some experiments carried out at 4.7 T, a Look-and-Locker-type sequence consisting of 20 FLASH images acquired immediately after a non-selective adiabatic inversion pulse (51, 179), was used for measuring T_1 (**I**).

On-resonance $T_{1\rho}$ was quantified using a spin-lock pulse of variable amplitude of (B_1 range 0.2-1.6 G determined across the imaging slice by calibrating the power needed to

produce 180 degree pulse of respective length). The spin-lock sequence consisted of two adiabatic half-passages, joined by a spin-lock period of variable length (spin-lock time, SLT) followed by a crusher gradient (87) in front of a line-scan acquisition (**II, III**). Dispersion of $T_{1\rho}$ over a range of B_1 fields was quantified by using four spin-lock amplitudes (0.2-1.6 G) (**III**).

A set of T_2 images were acquired using a single spin-echo sequence with either an BIR-4 refocusing pulse (**I, IV**) or a line-scan sequence with 180° sinc pulses (**II, III**). Spin density was estimated from a single exponential fit of T_2 MRI data acquired with multiple TEs and correcting for T_1 saturation effects (**I**). Spin density ratio between ischaemic and non-ischaemic hemispheres was estimated.

MTR was assessed by measuring signal intensity with (M_{sat}) and without (M_0) an off-resonance saturation pulse (**III**).

4.7.4 Relative CBV (CBV_{rel})

Changes in CBV were determined using an iron oxide based blood pool MRI contrast agent, (AMI-227, 6 mg/kg i.v., Guerbet, France) (**II, III, IV**) and the established linear relationship between the relaxation rate change (ΔR_2) and contrast agent concentration (227). Relaxation data was obtained using a SE pulse sequence. Hematocrit was assumed to remain constant.

$$\Delta R_2 \propto C(t)CBV \qquad [17]$$

ΔR_2 was obtained from T_2 values prior to and after injection of AMI-227

$$\Delta R_2 = \frac{1}{T_{2,post}} - \frac{1}{T_{2,pre}} \qquad [18]$$

AMI-227 has a half-life of >4 hours in the rat (194). In the KCl induced global ischaemia experiments (**III**), the delay from AMI-227 injection to cardiac arrest was about 20 minutes, and the washout of the contrast agent was not corrected for. In other experiments (**II, IV**), the total measurement time was more than an hour, and consequently, the decay of intravascular contrast agent was corrected to avoid underestimation of CBV. A corrected ΔR_2 at each time point (elimination time constant, λ, 0.154 h^{-1}, t in hours) (194) was calculated according to

$$\Delta R_{2,corr}(t) = \Delta R_2(t)e^{\lambda t} \qquad [19]$$

The relative CBV (CBV_{rel}) changes were computed from the equation

$$CBV_{rel} = \frac{\Delta R_{2,corr}(t)}{\Delta R_{2,corr}(0)} \qquad [20]$$

The effect of AMI-227 on the parenchymal $T_{1\rho}$ and T_2 was quantified by injecting the contrast agent i.v. in a step-wise manner up to a level of 16 mg/kg.

4.7.5 Intracellular pH (pH_i) and energy status: ^{31}P NMR spectroscopy

Surface-coil localised ^{31}P NMR spectra were acquired using a pulse-acquire-sequence (**II**) and PCr, free inorganic phosphorus P_i, and ATP peaks were fitted using the Advanced method for

accurate, robust and efficient spectral fitting [AMARES, (249)] in the Java version of the Magnetic Resonance User Interface [MRUI (175, 241), www.mrui.uab.es/mrui/]. pH_i was calculated from the chemical shift difference between PCr and P_i peaks using calibration curve by Taylor et al. (226).

4.7.6 Tissue temperature, lactate concentration and pH_i: ^1H NMR spectroscopy

Non-water-suppressed ^1H NMR spectra were acquired using a stimulated echo acquisition mode (STEAM) sequence (69) with a localised 8x8x4 mm^3 voxel positioned in the area covering both putamen and parietal cortex (**III**). Spectra were collected prior to ischaemia and 20 minutes after induction of global ischaemia in animals with varying pre-ischaemic blood glucose levels.

Water, choline-containing metabolites, creatine+PCr, N-acetyl aspartate (NAA) and lactate (only in the ischaemic brain) were fitted using a Variable projection method (VARPRO) (129) in Matlab version of MRUI. Brain temperature was calculated from the frequency difference between water and NAA utilizing the quantitative interrelationship determined by Cady et al. (34). Fitted signal amplitudes were used to calculate absolute lactate concentration. Intracellular pH (pH_i) was calculated from brain lactate using an established relationship taking into account pre-ischaemic pCO_2 status (124).

4.7.7 Blood $T_{1\rho}$ and T_2

NMR relaxation times $T_{1\rho}$ and T_2 were determined in a fresh bovine blood thermostated to 37°C (**II**). Oxygen saturation was adjusted by mixing N_2 and O_2, each containing 5 % CO_2, in a gas exchange system as previously described (78). Blood was circulated in a cuvette (diameter of 8 mm) positioned vertically and perpendicular to B_0. The effect of reduced pH on blood $T_{1\rho}$ MR relaxation was also explored by reducing pH from 7.30±0.04 to 6.90±0.01 while maintaining oxygen saturation >0.95.

Blood $T_{1\rho}$ and T_2 were determined also in the presence of AMI-227 in heparinised rat blood by increasing the contrast agent concentration up to 200 mg/µl (approximates to an injection of 12 mg/kg in a 350 g rat). These experiments were carried out in well-mixed blood samples at room temperature.

4.7.8 Relaxation in BSA solutions

Bovine serum albumin (BSA, fraction V, Sigma Chemicals, St. Louis, MO) was dissolved in potassium phosphate buffer (pH 7.4) to yield an 8% solution (**II**). The dissolved gas content in the phantoms was manipulated before sealing the samples in 5 mm NMR tubes as follows: (i) nominal zero dissolved gas was obtained by freezing and thawing the samples in a vacuum, (ii) room air-saturated samples were frozen and thawed under normal air pressure, and (iii) samples were equilibrated with 100% oxygen for 15 minutes. Relaxation times were determined spectroscopically as described previously (172).

4.7.9 Data analysis

Absolute T_2, T_1, $T_{1\rho}$ and diffusion images were computed by fitting the data to a single-exponential as a function of TE, TI, SLT and b-values, respectively. T_1 FLASH data obtained with the Look and Locker method were analysed taking into account the effect of FLASH acquisition to the relaxation curve as described by Nekolla et al. (179). MRI parameters during insult were compared with control values obtained from control hemisphere (focal ischaemia) (**I**) or prior to ischaemia (global ischaemia) (**I-IV**) or hypoxia/hypercapnia (**II**). Statistical significance was analysed using Student's t-test and one-way analysis of variance (ANOVA) with Tukey's honest significant difference post-hoc test (level of significance at $p<0.05$).

The dependence of $T_{1\rho}$ on spin-lock field amplitude, termed as $T_{1\rho}$ dispersion, was estimated using an exponential fit of the format (87)

$$T_{1\rho} = -Ae^{-B1} + B \qquad [21]$$

Fitted coefficients, A and B, can be interpreted so that A describes the $T_{1\rho}$ dispersion ($d_{T1\rho}$) while B-A estimates $T_{1\rho}$ as B_1 approaches zero. This empirical procedure has been shown to provide a good estimate for *in vivo* $T_{1\rho}$ values acquired with different B_1 amplitudes (87). However it should be noted that the computations were used to facilitate the comparison of dispersion changes rather than for a rigorous treatment of $T_{1\rho}$ data. $\Delta d_{T1\rho}$ in ischaemic tissue was calculated as the relative change of coefficient A as compared with the same brain area prior to the insult.

The kinetics of MRI variables following cardiac arrest was analysed by estimating the time points where the change in $T_{1\rho}$ and D_{av} started (t_{ini}) and 50% of the maximal change had occurred (t_{50}). For this purpose $T_{1\rho}$ and D_{av} were fitted to equations

$$X(t) = X_0 \qquad t<t_{ini} \qquad [22a]$$

$$X(t) = X_0 + D\left[1 - e^{\frac{-t-t_{ini}}{C}} + k(t - t_{ini})\right] \qquad t>=t_{ini} \qquad [22b]$$

Fitted values for t_{ini}, X_0 (a value prior to KCl injection), C (an exponential term for initial rapid change), k (a linear term mainly corresponding to slower change in the later phase) and D (a scaling factor for the overall magnitude of the change) were used to calculate t_{50}.

4.7.10 Simulation of parenchymal T_2 and $T_{1\rho}$ relaxation times

A model quantitatively relating SE BOLD changes with physiological parameters including CBF, $CMRO_2$, CBV and OER (247) has previously been successfully applied to several haemodynamic challenges including acute hypoperfusion and ischaemia (88, 125), hypoxia (247) and hypercapnia (237). In the following section, the key equations and quantitative assumptions of the theory relevant to the current experimental settings (**II**, **IV**) are summarised. The same intravascular T_2 BOLD model with minor modifications was used for

estimation of parenchymal $T_{1\rho}$ changes, since the MRI timing of $T_{1\rho}$ and T_2 experiments are very similar.

An MRI voxel contains tissue and a mixture of blood vessels with different oxygenation levels (arterioles, capillaries and venules). Therefore the contribution of both blood and tissue R_2 (or $R_{1\rho}$) has to be accounted for in calculating parenchymal relaxation effects. As a slow exchange of water between microvessels and tissue (193) is expected to prevail also in ischaemia as long as the blood brain barrier is intact, the signal attenuation in a SE experiment can be expressed as:

$$\frac{M(TE)}{M(0)} = x_{tissue} e^{-R_{2,tissue} TE} + \sum_i x_{blood,i} e^{-R_{2,blood,i} TE} = e^{-R_{2,app} TE} \quad [23]$$

in which *a, c* and *v* indicate arteriolar, capillary and venular volumes, respectively. The tissue fraction (x_{tissue}) and blood fractions ($x_{blood,i}$) are related via

$$x_{tissue} = 1 - \sum_i x_{blood,i} = 1 - \sum_i \frac{CBV_i}{V_d + CBV - CBV_{norm}} \qquad i \in a,c,v \quad [24]$$

where V_d (in µl/g) refers to the normal brain water distribution volume [820 µl/g (211)] and CBV_{norm} (in µl/g) to the CBV under normal conditions [4.77±0.13 % (207)]. To estimate the combined effect of all the different microvessels, the functional arteriole:capillary:venule volume ratio of 0.05:0.49:0.46 was used, where the capillary fraction includes capillaries and smaller arterioles where the gas exchange occurs (88, 214).

The R_2 in blood can be derived as volume-weighted sum of the relaxation rates in different compartments (247):

$$R_{2,blood,i} = Hct_i R_{2,ery} + (1 - Hct_i) R_{2,plas} + Hct_i (1 - Hct_i)(\Delta\omega_i)^2 \tau_i \left[1 - \frac{2\tau_i}{\tau_{CPMG}} \tanh\left(\frac{\tau_{CPMG}}{2\tau_i} \right) \right] \qquad i \in a,c,v \quad [25]$$

where $R_{2,ery}$ and $R_{2,plas}$ are the relaxation rates for erythrocytes and plasma, respectively, $\Delta\omega_i$ is the susceptibility difference and τ_t is the lifetime of exchange of water between plasma and erythrocytes, Hct is cerebral microvascular hematocrit [the values for the five above-mentioned parameters were taken from (88)] and τ_{CPMG} is the interpulse interval in a Carr-Purcell-Meiboom-Gill (CPMG) multiecho method (88, 247). $\Delta\omega_i$ is determined by the fraction of the deoxygenated haemoglobin (x_{deoxy}) that in turn depends on the arterial oxygen saturation fraction (Y_a) and OER and can be expressed in microvessels as

$$x_{deoxy,a} = 1 - Y_a \quad [26a]$$

$$x_{deoxy,c} = 1 - Y_a + 0.5 \cdot OER \cdot Y_a \quad [26b]$$

$$x_{deoxy,v} = 1 - Y_a + OER \cdot Y_a \quad [26c]$$

$$OER = \frac{CMRO_2}{[Hb_{tot}] \cdot CBF \cdot Y_a} \quad [27]$$

where $[Hb_{tot}]$ is the haemoglobin concentration (247). It should be noted from eq. [25] that in the CPMG experiment where there is a very short interpulse interval and a large number refocusing pulses, the exchange contribution becomes negligible, leading to lower sensitivity of these sequences to BOLD (247). In contrast, in the Hahn single echo method with τ_{CPMG}=TE, the exchange effects become maximal resulting in a large BOLD effect with single echo MRI as well as in a TE dependency of T_2 (29). Consequently, parenchymal T_2 must be determined from data acquired with several TE times from high signal-to-noise ratio images for quantification of BOLD. To determine the fractional contribution of blood to the parenchymal $T_{1\rho}$, blood relaxation can be estimated from calibration curves of blood $T_{1\rho}$ as a function of oxygen saturation (**II**).

Experimental data from cerebral ischaemia show that the R_2 of the tissue remains unaltered after short periods of ischaemia (128, 144). The relaxation rate for the rat cerebral tissue ($R_{2,\,tissue}$) at 4.7 T was determined from control data using OER of 0.36 under normal physiological conditions (247).

5 RESULTS

Physiological values including arterial blood gases, blood glucose, MABP and core temperature were close to normal during the experiments (**I-IV**). Hypoxic hypoxia, hyperoxia or hypercapnia (**II**) resulted in altered pO_2 or pCO_2 status, respectively, as desired. Similarly the blood glucose levels were significantly altered in the rats injected with insulin (hypoglycaemia group) or 50% glucose (hyperglycaemia group) (**III**).

Table 2. Quantitative MRI data from normal rat brain at 4.7 T

Article	T_1 (ms)	T_2 (ms)	$T_{1\rho}$ (ms)	MTR[A]	D_{av} ($10^{-3}mm^2/s$)
I	1459±11	n.d.	n.d	n.d.	0.74±0.01
II	1390±40	51.7±0.5	78.5±0.6 (B_1=0.6 G)	n.d.	0.77±0.01
III	n.d	56.8±0.4	101.0±0.5 (B_1=1.6 G)	0.60±0.05	0.74±0.01
IV	n.d.	51.3±0.6	n.d.	n.d.	0.70±0.02

Values are as means±SEM. [A]Pulse length 5 s, B_2 amplitude 0.3 kHz, 6 kHz off-resonance.
n.d. not determined

5.1 Parenchymal relaxation in hypoxic hypoxia, hyperoxia and hypercapnia (II)

Parenchymal MR relaxation is sensitive to chemical exchange and (paramagnetic) susceptibility effects. The contributions of acidosis through pH dependent proton exchange and intra- and extravascular susceptibility to parenchymal $T_{1\rho}$ relaxation were quantified in energetically competent brain tissue by (i) inducing tissue acidification by hypercapnia and (ii) by altering PtO_2 with hypoxic hypoxia and hyperoxia.

During severe hypercapnia, a reduction of pH_i by 0.3 was associated with an increase in $T_{1\rho}$ by 2.9±0.1 ms, as measured with B_1 field of 0.6 G. Using the blood $T_{1\rho}$ relaxation data and the intravascular BOLD model, it was estimated that 50% of the response could be due to the haemodynamic adaptations to hypercapnia. The computed values were in agreement with the data from the rats injected with AMI-227 showing an increase in parenchymal $T_{1\rho}$ of 1.8±0.3 ms upon severe hypercapnia. Under these conditions, the blood $T_{1\rho}$ had been shortened below 10 ms thus giving negligible contribution from the vascular compartment to the parenchymal $T_{1\rho}$ relaxation. The plots of parenchymal $T_{1\rho}$ determined either in the presence or absence of AMI-227 vs. pH_i suggest that an acidification of cerebral pH_i by one pH unit would prolong tissue $T_{1\rho}$ approximately by 4-5%.

Molecular oxygen is a well-known paramagnetic agent (40). In line with this, both T_1 and $T_{1\rho}$ were shorter in BSA phantoms equilibrated in the 100% oxygen atmosphere than in degassed protein solutions. In the brain parenchyma during hyperoxia with a PtO_2 of ~60 mmHg, T_1 was 1.8% shorter than in normoxic brain. Since hyperoxia is known not to influence cerebral haemodynamics (254), this T_1 response may be a direct consequence of the high tissue oxygen content. Parenchymal $T_{1\rho}$ was unchanged both in hyperoxia and hypoxic hypoxia, despite a 19% increase in CBV during the latter condition. Taking into account the measured blood $T_{1\rho}$ in hypoxic animals, this effect alone would shorten parenchymal $T_{1\rho}$ by

0.6% as computed using the model. Since no significant change in hypoxic brain was observed, it appears that the effects of negative BOLD and PtO_2 of ~25 mmHg on brain $T_{1\rho}$ are too small to be detected.

These data showed that parenchymal $T_{1\rho}$ relaxation is influenced by pH_i and macroscopic susceptibility effects, but is apparently not sensitive to microscopic susceptibility via PtO_2.

5.2 Parenchymal relaxation times following cardiac arrest (I-III)

The model of global ischaemia induced by cardiac arrest is very useful for studies of a haemodynamic condition with no residual blood flow and, if induced with KCl injection, also with small CBV (47). These haemodynamic conditions allow for MRI determination of a relatively pure tissue response to ischaemia, bearing in mind the possible effect of residual CBV.

The observed changes in diffusion were consistent with previous reports from normocapnic, normoxic and normoglycemic rats, where there is a large decline in water diffusion starting about 50 seconds after cardiac arrest preceded by a small (~5%) drop in diffusion (Fig. 3) (43, 46, 47, 50, 103, 116).

T_1 was prolonged immediately after cardiac arrest, clearly preceding the large diffusion change. By 100 seconds, T_1 levelled off to values that were 4-7 % higher than controls. The increase in T_1 was present at 1.5, 4.7 and 9.4 T both in cortical and striatal brain (**I**).

A drop in single-echo T_2 by 8% was evident after cardiac arrest and T_2 remained 5 % below the pre-ischaemic value for the observation period of 20 minutes. In the animals injected with AMI-227 prior to ischaemia, T_2 started to increase immediately, attaining a 20% longer level by 20 minutes of ischaemia. This corresponded to about a 40-50 % decrease in CBV, in agreement with a previous report (47). Since the blood T_2 in the animal receiving AMI-227 was <10 ms, these experiments confirm that the T_2 drop in the global ischaemia is due to negative BOLD effect (46, 47, 88).

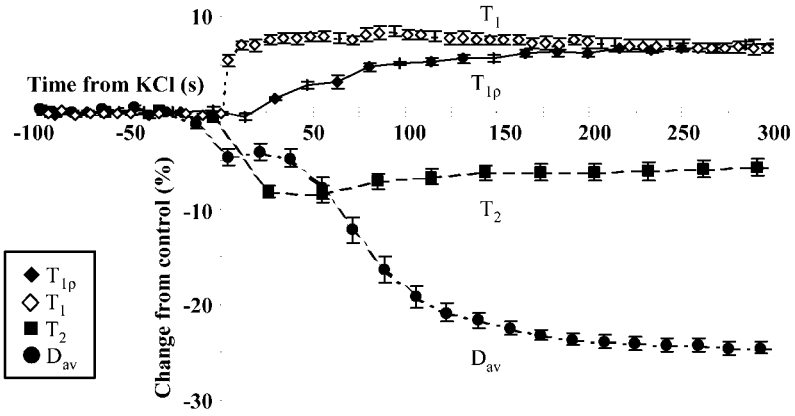

Fig. 3. Changes in cerebral MR parameters following cardiac arrest in normoglycemic animals at 4.7 T (**I**, **III**).

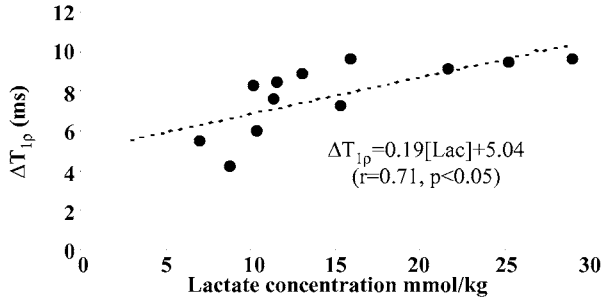

Fig. 4. $T_{1\rho}$ change after 20 minutes of global ischemia in animals with varying tissue lactate levels.

$T_{1\rho}$ acquired with a B_1 field of 1.6 G began to increase after 10-20 seconds of ischaemia, kinetics that was clearly distinct from the T_1 response (**III**). After 200 seconds, the increase in $T_{1\rho}$ levelled off to a value that was ~5 % greater than the pre-ischaemic value. The $T_{1\rho}$ increase started sooner than either the decline in tissue water diffusion or the anoxic depolarisation. The kinetics of $T_{1\rho}$ in global ischaemia was virtually independent of pre-ischaemic blood glucose level within the range from 1.7 to 29 mmol/l. In contrast, both diffusion and anoxic depolarisation were modulated by pre-ischaemic blood glucose so that the responses were expressed sooner at a low blood glucose level. Interestingly, the time courses of diffusion decline and anoxic depolarisation did not match, suggesting that water diffusion was reduced in the tissue before the loss of ionic homeostasis (103, 116). $T_{1\rho}$ dispersion, as determined from data collected with B_1 fields of 0.2, 0.6, 1.2 and 1.6 G, increased shortly after cardiac arrest, reaching values some 30% above control by 20 minutes of global ischaemia. Ischaemic $T_{1\rho}$ behaved similarly in the presence of AMI-227 contrast agent, when the contribution of blood was minimal. A plot of $\Delta T_{1\rho}$ vs. lactate concentration reveals the positive correlation between the two variables in the steady-state ischaemic conditions (Fig. 4). Using the established pH_i/lactate interrelationship (124), the volume-averaged cerebral pH_i was 6.5, 6.3 and 6.0 in hypo-, normo- and hyperglycaemic rats, respectively.

Magnetisation transfer was assessed in the brain tissue by means of computing MTR. Global ischaemia resulted in a drop of both M_0 and M_{sat}, an effect caused by rapid T_2 shortening. Importantly, the MTR figures did not change during the first minutes of ischaemia, but a time-dependent downward trend was evident in the slope of MTR values (**III**).

5.3 T_1 relaxation in rat focal ischaemia model with reperfusion (I)

Increased T_1 was observed within 8 minutes of MCAO in both ischaemic cortex and striatum, the difference in T_1 between ischaemic and non-ischaemic volumes increasing over time. D_{av} was severely reduced in both brain regions. Diffusion fully recovered upon retraction of the occluder after 20 minutes of MCAO in both tissue types in all animals studied, however, only a partial return of T_1 towards the level determined in the non-ischaemic hemisphere was

evident. After the initial sharp drop, T_1 did not change significantly in cortex while in striatum, an increasing trend was observed after the insult. These data indicate that in the focal ischaemia model where there is inevitable residual collateral flow, acute ischaemia is associated with an increase in T_1, however, this increase appears to be only partial upon reperfusion with normal diffusion. Since CBF was not determined in the ischaemic volume, the possibility that flow did not completely recover cannot be excluded. This is due to the fact that normal diffusion is maintained above CBF of 25 ml/100g/min, and thus CBF in the post-ischaemic volume might have been only partially restored leading to altered T_1.

Retraction of the occluder following 90-minute MCAO lead to either a complete recovery of D_{av} or to no recovery. In the former group of animals, a partial reduction of T_1 was observed upon reperfusion, while in the latter group T_1 continued to show an increasing trend. Spin density did not show any consistent changes during MCAO or reperfusion. Ischaemic T_1 changes did not appear to predict final tissue status as similar T_1 responses were observed both in apparently reversibly (20 minutes MCAO) and irreversibly damaged (90 minutes) cortex.

5.4 T_2 relaxation in the global ischaemia and subsequent reperfusion (IV)

The four-vessel vascular occlusion model used allows for controlling the degree of haemodynamic collapse as well as for performing the occlusion in the magnet bore. The goal of using this model was to quantitatively assess the recovery of brain haemodynamics and metabolism by MRI. This was undertaken (i) to understand the basic physiologic mechanisms and (ii) to study the MRI relaxation characteristics in association with ischaemia-reperfusion. Single SE T_2 MRI was employed to probe haemodynamic/metabolic variables owing to its sensitivity to BOLD using the intravascular model to determine the contributions of physiological factors. In the first phase of the study, CBF was gradually reduced for 15 minutes in one to three CBF levels per animals. One key observation from these experiments was that a positive BOLD response was present after release of occlusion only if CBF had dropped below 25% of control during the insult. This "threshold" is very close to that causing ischaemic energy failure and a drop in water diffusion, i.e. 20 ml/100g/min (33, 88). Since the postocclusion CBF did not show similar threshold pattern, the positive BOLD response may either be due to increased CBV or a reduced OER or a combination of these two factors.

To address the contributions of these physiologic mechanisms to BOLD, the four-vessel occlusion method was used to produce global ischaemia of either 7 or 15 minutes. During occlusion, residual CBF was <20% of normal and consequently, a severe drop in diffusion was detected. A shortening of T_2 relaxation time by 4-12% was determined in the early moments of ischaemia. Luxury perfusion was detected by the hydrogen clearance method after ischaemia and its duration was dependent on the length of ischaemia. Consistent with earlier reports (112), luxury perfusion was followed by a decline of CBF below the pre-ischaemic level. Prolongation of T_2 by about 10% was determined at the first time point both after 7 and 15 minutes of ischaemia, T_2 stabilising thereafter to the pre-ischaemic levels. CBV was

initially increased by about 30%, returning and stabilising to the control level by 15 minutes of reperfusion.

The MRI and haemodynamic data quantified from the brain immediately after ischaemia were used to estimate the contributions of haemodynamic (CBV) and metabolic (OER) factors to the BOLD. The computation, using the quantitative SE-BOLD model and the existing blood relaxation values, with the above data showed that the increase in CBV alone could explain 1/3 of the observed T_2 increase in post-ischaemic brain. This data indicate that the haemodynamic factors are only partially responsible for the BOLD occurring during luxury perfusion. Thus oxygen saturation of blood in the capillary/venular compartments during luxury perfusion must be very high. Indeed, the simulations show that OER in the order of 0.05 should prevail to account for the post-ischaemic T_2 BOLD. This suggests that $CMRO_2$ remains depressed during the first minutes of reperfusion. This conclusion is consistent with the invasive studies showing that metabolic recovery proceeds with delayed kinetics relative to that of haemodynamics (218).

6 DISCUSSION

6.1 The animal models

Several kinds of animal models have been used in the present work to perturb physiological homeostasis or to constrain the blood supply to the brain for mechanistic studies of MR relaxation times. Most of these rat models have been commonly used to obtain the desired perturbations, however, from a MR contrast generation point of view it is seldom possible to influence one specific physiologic or pathologic factor alone. It is therefore rather difficult to pinpoint the contribution of a given pathophysiological process to the MRI relaxation or diffusion of cerebral water. In an effort to separate the plausible effects of given physico-chemical factors on relaxation *in vivo*, one must accomplish a perturbation *in vivo*, say a pH_i change, without influencing the system as a whole. This can be obtained by respiratory acidosis that efficiently acidifies the cell interior without perturbing brain energetics. In hypercapnic animals, the effects of low pH_i on tissue relaxations can be explored, however, severe haemodynamic adaptations to the condition inevitably alter parenchymal relaxation times. Similarly, the level of inspired oxygen conveniently modulates PtO_2, yet contributions of haemodynamic factors in hypoxic hypoxia are present. In the present work, experimentally measured *in vivo* and *in vitro* relaxation data and the modelling of parenchymal relaxation (247) were combined in order to estimate the effects of vascular and tissue factors to MR relaxation times. These procedures were considered to yield novel conclusions from relaxation in the brain during the ischaemic insult. This approach has recently been applied for the single SE T_2 data from acute hypoperfusion to assign the negative BOLD effect entirely to intravascular phenomenona (88) demonstrating that modelling of T_2 BOLD is a powerful way of assessing tissue viability under compromised flow conditions (86).

6.2 MRI methodology

The T_1 and T_2 MRI relaxation times were quantified with standard methods and the figures obtained for the cerebral NMR relaxation agree well with reported values (35, 87, 89, 108, 155). One important factor affecting T_1 is the choice of the transmit rf coil. This is because the degree of inversion of blood water spin would certainly differ between scans acquired with the volume coil extending to the heart and a surface coil covering the head. In the former case, an IR method with a non-selective inversion pulse results in negligible sensitivity of T_1 to flow, whereas in the latter case an unavoidable contribution of flow remains. The flow effect was carefully evaluated in the present work. Single echo T_2 method used throughout the work has an inherent sensitivity to exchange related dephasing, making it maximally sensitive to BOLD, as well as the common features of inherent spin-spin relaxation and diffusion. This effect is very important if the data should be compared to data acquired with a CPMG method, since the latter technique shows a τ_{CPMG} –dependent sensitivity to BOLD and would give a different perspective of T_2 changes, for instance in acute ischaemia.

$T_{1\rho}$ MRI is also affected by the type of coil due to its inherent sensitivity to the B_1 homogeneity. This is because the relaxation takes place in the rotating frame generated by the rf coil and in the presence of rf field inhomogeneities, the effective field (and the effective frequency, ω_{eff}) sensed by the spins varies leading to dispersion of relaxation times

$$\omega_{eff} = \sqrt{\omega_1^2 + \Delta\omega^2} \qquad [28]$$

where $\omega_1 = \gamma B_1$ and $\Delta\omega = \omega_{sl} - \omega_0$, the difference between the Larmor frequency and the spin-lock frequency, is determined by both the residual local fields and the varying rf field. Only in conditions where $\omega_1 >> \Delta\omega$, does the magnetisation remain spin-locked (201). Therefore in the $T_{1\rho}$ MRI with B_1 inhomogeneity, the relaxation time may spatially vary because of ω_{eff} variation. In the $T_{1\rho}$ experiments with the surface coil in the transmit mode, this is a potential source of artifact. In the present work, an adiabatic pulse was used to minimise the sensitivity of pulse sequence for the B_1 inhomogeneity, and the imaging slice was selected in the most homogenous part of the coil as judged from the pilot MRI. Indeed, no significant variation in absolute $T_{1\rho}$ was evident acquired with a B_1 range of 0.2 to 1.6 G. This directly shows that the rf inhomogeneity was not a confounding factor for $T_{1\rho}$ quantification *in vivo*.

6.3 Effects of pH on brain $T_{1\rho}$ relaxation

The present data strongly argue for a direct effect of intracellular acidosis on tissue $T_{1\rho}$ relaxation in the energetically viable brain. It is evident that hypercapnia, used to produce intracellular acidosis, is associated with an increase in CBF and CBV (84, 254) that affects parenchymal T_2 and $T_{1\rho}$ relaxation. The BOLD contribution to parenchymal $T_{1\rho}$ can be computed by applying the formulas of the intravascular T_2 BOLD model (247). The calculations show that about 50% of parenchymal $T_{1\rho}$ response to severe hypercapnia is due to vasculature, the other half arising from tissue. This estimate agrees well with the cerebral $T_{1\rho}$ value determined in the hypercapnic animals injected with AMI-227 to remove the blood contribution from the parenchymal MRI.

The increase in tissue $T_{1\rho}$ upon acidification is not unexpected based on the protein phantom studies demonstrating a slow down of the $T_{1\rho}$ relaxation rate at low pH. The physico-chemical mechanism mediating the effect is the proton exchange, i.e. exchange of labile protons of macromolecular –OH, -NH, -SH (59, 192, 260) or amide groups (166) with bulk water protons. Since it is a base-catalysed process, proton exchange is inhibited at low pH leading to protonation of these side chain groups. Mäkelä et al. (172) have recently shown that both in native and heat denatured immobilised protein phantoms, both showing ^{1}H NMR peaks from exchangeable protons; proton exchange is the dominant relaxation mechanism for $T_{1\rho}$ at a B_1 field range from 0.2 to 2.6 G. The exchange rate for the side chain protons is in the order of 10^2-10^4 s^{-1} (145, 260), a rate that matches well with the "resonance" condition imposed by B_1 fields used in $T_{1\rho}$ data acquisition. On the other hand the contribution of molecule exchange to $T_{1\rho}$ in protein phantoms may be small (172). This is important, since the

molecule exchange is the dominant mechanism mediating MT *in vivo* (106). Interestingly, ischaemic MT and $T_{1\rho}$ change apparently independent of each other in the early moments of both global (**III**) and focal ischaemia (173).

6.4 Effects of macroscopic and microscopic susceptibility on parenchymal $T_{1\rho}$

Blood and protein phantom results show that BOLD or/and dissolved oxygen influence $T_{1\rho}$. The BOLD effect on $T_{1\rho}$ is linear in nature, differing from the behaviour of single SE T_2. The difference may reflect the fact that the spin-lock MR is inherently less sensitive to the susceptibility effects than a spin-echo method. Parenchymal $T_{1\rho}$ did not change during hyperoxia suggesting that the concentration range at which molecular oxygen directly shortens $T_{1\rho}$ may be higher than attainable *in vivo*.

The low blood oxygen saturation level does not influence parenchymal $T_{1\rho}$ in hypoxic hypoxia. This observation is consistent with the data from a hypoperfusion model and reveals the inherently low sensitivity of $T_{1\rho}$ to "true" BOLD (87). Therefore, the susceptibility gradients by deoxyhaemoglobin under these conditions affecting T_2*, apparently are not sensed by the rotating frame relaxation *in vivo*. Likewise, the tissue paramagnetic effects by dissolved oxygen are too small to be detected by $T_{1\rho}$. These conclusions are important in the interpretation of $T_{1\rho}$ behaviour in the ischaemic brain, since it appears that the endogenous paramagnetic susceptibility effects prevailing under any condition *in vivo* are too small to influence parenchymal $T_{1\rho}$.

6.5 Pathophysiological effects on the MR relaxation in hyperacute cerebral ischaemia

Evidently, substantial changes in T_1, $T_{1\rho}$ and T_2 take place in the parenchyma within the very first minutes of ischaemia. Ischaemic T_2 changes have recently been explained by an intravascular negative BOLD effect (35, 86, 88, 89) and the present data is consistent with this conclusion. However, the pathophysiologic factors causing the immediate T_1 increase (**I**) require a thorough discussion. The data indicate that cessation of flow as such is one of the major factors lengthening T_1. There are several observations favouring this conclusion. The kinetics of the relaxation time is very fast, in fact the T_1 change precedes the response of any other MRI variable studied, and the collapse of flow upon cardiac arrest resembles the T_1 increase. Furthermore, one can estimate that cessation of CBF of 100 ml/100g/min would prolong parenchymal T_1 by 2-4% matching reasonably well the measured change. One factor that has to be considered here is the water exchange between blood and tissue. Under physiological conditions the water lifetime in the capillaries is 500-1000 ms (193), thus considerable exchange between the water pools occurs during T_1 measurement (57, 266). The exchange processes may become influenced by cessation of CBF, leading to altered T_1 relaxation. The separation of different mechanisms is complicated, however, by the fact that due to the time scale of the T_1 measurement (in the order of seconds), the exchange is in the slow-intermediate regime (266). On the other hand, the data also suggest that PtO_2 can

influence cerebral T_1 and thus exhaustion of oxygen may well contribute to the immediate relaxation change. Furthermore, differential field-dependency of cortical and striatal T_1 in hyperacute ischaemia argue in favour of a tissue type related effect suggesting that there is an altered microenvironment of tissue water. The results show that the plausible microenvironmental effect may not involve a MT change.

In the global ischaemia model evoked by cardiac arrest, net accumulation of water is impossible and therefore, the T_1 increase depicted above is certainly independent of tissue water content. This conclusion is evidently applicable also in the early moments of the focal ischaemia, where a 5-7% prolongation of T_1 was detected at 4.7 T without any signs of a spin density increase. The association of diffusion and T_1 immediately after retraction of the occluder thread favour the hypothesis of direct flow contribution to the MR relaxation. The present data show incomplete recovery of T_1 during reperfusion and this may either be due to an incomplete restoration of flow and/or persistently defective water communication in the post-ischaemic brain. It appears that the kinetics of T_1 recovery after focal MCAO is not a predictive MRI index for the long-term tissue outcome, suggesting that the factors influencing initial T_1 changes are dynamic in their nature. Further experiments are needed to estimate the application of T_1 in hyperacute stroke.

One of the key observations in the current studies is that the parenchymal $T_{1\rho}$ indicates global ischaemia simultaneously or even slightly earlier than diffusion MRI. The spin-lock method employing non-selective adiabatic spin-lock is evidently not directly sensitive to flow and in line with this observation, it takes some 10-30 seconds of ischaemia before $T_{1\rho}$ begins to become prolonged. Therefore, cessation of flow as such may not contribute to the prolongation of $T_{1\rho}$ (87). The time courses for exhaustion of PtO_2 and expression of negative BOLD match reasonably well with the $T_{1\rho}$ kinetics. The quantitative MR data from phantoms with varying amounts of dissolved O_2 *in vitro* and direct manipulation of O_2 *in vivo* demonstrate negligible direct effect of molecular oxygen at the physiological concentration range of PtO_2 on $T_{1\rho}$. $T_{1\rho}$ evidently detects BOLD *in vitro* and *in vivo*, however, the sign of the BOLD effect is opposite to that determined by $T_{1\rho}$ in ischaemic brain. Similarly, the data from intravascular contrast agent experiments suggest that the macroscopic susceptibility contribution to the ischaemic relaxation is small. Thus, it appears that neither of these factors affecting susceptibility can explain the hyperacute $T_{1\rho}$ increase. One important conclusion to be drawn from the BOLD and AMI-227 data is that the $T_{1\rho}$ change in hyperacute ischaemia must take place predominantly within the tissue.

Tissue water $T_{1\rho}$ relaxation and diffusion show distinct time courses in global ischaemia and therefore, the decline of the conventional diffusion of bulk water does not directly provoke the ischaemic $T_{1\rho}$ increase. The common hypothesis of ischaemic diffusion decline claims that the shift of water from extracellular environment into the restricted intracellular space would account for the early diffusion drop. This hypothesis has been recently challenged on theoretical (220) and experimental (58, 96, 103, 178) grounds. Simultaneous measurements

of diffusion and DC potential demonstrate a large diffusion drop before anoxic depolarisation occurs. Since the collapse of ECS size (and thus water movement into cell interior) coincide with depolarisation, any major delay in the DC potential change relative to the collapse of diffusion suggests that water movement into cell interior does not directly initiate the decline in diffusion. The data thus argue against the causal relation of anoxic depolarisation with the diffusion drop. As far as $T_{1\rho}$ is concerned, ionic and water movements are apparently not responsible for changes seen in hyperacute ischaemia.

Cerebral $T_{1\rho}$ is evidently influenced by pH_i in energetically viable tissue. Therefore the inevitable acidification of brain, starting within minutes from the onset of ischaemia (124, 180), is a potential contributing factor to cerebral $T_{1\rho}$ through changes in proton exchange (59, 159, 172, 255, 265). Interestingly, the reported CBF threshold of ~20 ml/100g/min for the cerebral $T_{1\rho}$ increase (87) is close to that of ischaemic acidification (42, 95). Furthermore, an association between ischaemic lactate and $T_{1\rho}$ at steady state supports this view. However, the data suggests that low pH_i may contribute to the prolonged MR relaxation only after the initial increase. The direct comparison of $T_{1\rho}$ and pH_i changes with high temporal resolution was not determined in the current study. However, data for the kinetics of lactate accumulation and pH_i, determined in the same animal model (50, 124), indicate that the significant lactate build-up begins after a time lag of 60-90 seconds of cardiac arrest. Similarly, several laboratories have determined the kinetics of pH in ECS (pH_e) in global ischaemia, and pH_e has an established link to pH_i. These data show that pH_e starts to decline after 60-90 seconds of ischaemia, thus following the kinetics of lactate generation. Indeed, Katsura et al. (124) have shown that the magnitude of pH_e acidification is determined by anaerobic lactate production, however, the initial acid shift may be independent of lactate accumulation. Taking these data into account, it is concluded that during evolution of ischaemia acidosis is associated with tissue $T_{1\rho}$ yet tissue acidification may have a time course that is too slow to explain the $T_{1\rho}$ increase in hyperacute ischaemia.

Pre-ischaemic blood glucose evidently determines the capacity of anaerobic glycolysis to yield ATP (215). Despite the inefficiency of glycolysis to harvest ATP, the anaerobically produced ATP maintains membrane polarisation for a substantial period after induction of ischaemia. In the light of this observation, it is interesting that cerebral $T_{1\rho}$ in ischaemia is apparently not maintained by anaerobic metabolism. The present data suggest that inhibition of oxidative metabolism evokes perturbations in the cellular homeostasis that alter tissue $T_{1\rho}$ in ischaemia. This claim is supported by the fact that PtO_2 is exhausted independent of blood glucose status and thus mitochondrial ATP synthesis ceases within 10-30 seconds of ischaemia (151, 158, 174). Inhibition of mitochondrial respiration is associated with marked reductions of the electron carriers and thus water in the vicinity of mitochondria may experience altered susceptibility in the ischaemic tissue. Altered magnetic susceptibility in the ischaemic tissue may influence $T_{1\rho}$ through an effect on the ω_{eff} as explained above.

It is firmly established that chemical exchange has an inevitable effect on MRI contrast. The present data show that MT, commonly believed to be mediated through dipolar coupling and cross-relaxation (106), does not change in the early phase of global ischaemia. This observation is consistent with reports showing that the MR rate declines only hours after permanent (64, 190) or transient (173) focal cerebral ischaemia. It has been proposed that the magnetisation transfer rate declines due to water accumulation and it is not therefore surprising that the MT contrast responds only to irreversible ischaemia. These observations together with the present results suggest that MT and $T_{1\rho}$ probe different physico-chemical mechanisms *in vivo*.

From the discussion above, it can be concluded that several pathophysiologic factors potentially contribute to the increase in tissue $T_{1\rho}$ due to acute ischaemia. The current studies suggest that ionic and water shifts associated with anoxic depolarisation do not significantly contribute to tissue relaxation change. In contrast, developing acidosis is likely to be involved in the ischaemic $T_{1\rho}$ change. Furthermore, the fast kinetics of the change point to a role of inhibition of respiration which potentially may either directly or indirectly influence tissue $T_{1\rho}$, but this hypothesis remains to be explored in the coming years. Nevertheless, it is concluded from the existing data that the altered tissue water microenvironment is the main cause for the hyperacute $T_{1\rho}$ response.

6.6 Potential applications of relaxation measurements in MRI of stroke patients

The relaxation time changes presented in previous studies (35, 87-90, 155) and the present work carry potential for providing complementary information about tissue status. The BOLD MRI methodology has established pathophysiologic correlations with acute ischaemia and it is therefore not surprising that it has attracted clinical attention. One limitation to the quantitative approach used in the present study is the model's sensitivity to $R_{2,tissue}$, a parameter difficult to measure using conventional methods. This complicates absolute quantification at later time points, as it is essential to account for the change in tissue relaxation due to developing oedema. This problem could possibly be circumvented, however, by studying relaxation in blood (78, 187) provided that a large vein can be located close to the ischaemic region. BOLD sensitive MRI techniques have already been employed in the assessment of oxidative metabolism of acute stroke patients using a standard 1.5 T clinical scanner (146). T_1 and $T_{1\rho}$ MRI do not yet have established pathophysiologic correlations, yet the lack of a full understanding of pathophysiologic mechanisms behind the contrast generation has not prevented clinical application of valuable MRI methods. This is best exemplified by diffusion MRI, which has had an enormous impact in the assessment of acute stroke patients, yet the mechanisms leading to diffusion contrast are still debated. In fact, preliminary $T_{1\rho}$ data from acute stroke patients has already been reported (213).

Several practical constraints and technical issues have to be dealt with prior to the application of T_2, T_1 or $T_{1\rho}$ in stroke patients. The changes observed in animal experiments are

relatively small in absolute relaxation times. At 4.7 T, the changes in relaxation times can also be observed by visual evaluation from respectively weighted images (eg. TE ~ T_2 would lead to 2-5% signal changes) provided that signal to noise ratio is high. However, for accurate quantification, the measurement of absolute relaxation times is required. At clinical field strengths, the situation appears to be different as virtually no changes in relaxation times have been reported within the first hours of ischemia (12). The different response may be due to field dependency of relaxation times (23, 62). For example, simulation of T_2-BOLD response to hypoperfusion indicates that changes are smaller at 1.5 T than at 4.7 T (88, 125). It is therefore possible that small changes in relaxation times are not accurately detected in routine signal analysis. This would mean in practical terms that absolute relaxation time images have to be acquired and constructed from the entire brain volume within a limited scan time of severely ill patients. This is technically feasible with a modern scanner within a couple of minutes, though all the current clinical equipment does not support tpe EPI-type of fast imaging methods. Interestingly, a recent study in stroke patients at 1.5 T reports signal reductions in T_2*-weighted images in the areas with compromised perfusion, suggesting that BOLD related signal changes are also clinically observable (224).

The estimation of the value of T_1 for the diagnosis and assessment of tissue status requires more work in the experimental settings. It is foreseeable that the ASL methods will be applied to acute stroke patients shortly to determine the state of perfusion, and with these methods also clinical experience of T_1 contrast will accumulate. Finally, $T_{1\rho}$ MRI does face an inherent problem of exceeding the specific absorption rate of energy (SAR) limits. Until the present, $T_{1\rho}$ contrast has been clinically used at low B_0 fields (up to 0.2 T) due to the SAR limitations. Since the rf deposit scales approximately to the second power of B_0 and B_1, only low spin-lock fields are applicable in humans at 1.5 T. In order to apply $T_{1\rho}$ MRI methods used in the present study to human imaging at equivalent field strengths, very long TR would have to be used making the methods impractical.

One recent observation towards the clinical applications of $T_{1\rho}$ MRI is that Carr-Purcell (CP) T_2 MRI contrast at 4.7 T may share many features of $T_{1\rho}$. It was shown that the Localization by adiabatic selective refocusing (LASER) CP method with short τ_{CP} (74) produces MR contrast akin to the $T_{1\rho}$ contrast in brain tumours at 4.7 T (O. Gröhn, unpublished data). The physical basis for the similar contrasts by LASER and $T_{1\rho}$ lies in the fact that at short τ_{CP}, the former method approaches the spin-lock condition and thus the contrast obtained receives contributions from the same physical factors as the on-resonance $T_{1\rho}$ (171, 208). The LASER method can be used in clinical settings without exceeding the SAR limits at 4.7 T thus making it a potential alternative to $T_{1\rho}$ MRI.

7 SUMMARY AND CONCLUSIONS

The present work demonstrates that subtle changes in T_1, T_2, and $T_{1\rho}$ MR relaxation times occur in the very early moments of cerebral ischaemia. T_1 and T_2 responses are mainly caused by haemodynamic and metabolic changes, respectively. The kinetics of ischaemic $T_{1\rho}$ change was distinct from those of diffusion changes and importantly, the former variable was not influenced by the pre-ischaemic blood glucose level. The data from hypercapnic animals suggest that acidosis may contribute to the prolonged tissue $T_{1\rho}$. Quantitative T_2 MRI applied during the early moments of reperfusion after global ischaemia shows a positive BOLD response with contributions from both haemodynamic and metabolic factors.

The following conclusions are drawn:

1. The MR relaxation times significantly change in the early moments of ischaemia. Pathophysiologic factors involving both haemodynamics and tissue underlie the altered parenchymal relaxations.

2. Combination of *in vivo* and *in vitro* experiments with modelling of parenchymal relaxation effects offer valuable tools for estimating contributing mechanisms.

3. The early T_1 response is mostly a result of reduced CBF.

4. $T_{1\rho}$ is among the earliest MRI markers of ischaemia, the effect taking place in tissue and involving changes in the physico-chemical microenvironment of water. The pathophysiologic mechanisms causing $T_{1\rho}$ are different from diffusion, indicating that these MRI parameters provide complementary information from the ischaemic brain.

5. Absolute T_2 BOLD MRI helps to evaluate haemodynamic and metabolic events both during and after ischaemia. The method can potentially be used in the assessment of metabolic recovery post-ischaemia.

8 REFERENCES

1. Abragam A. The Principles of Nuclear Magnetism. Oxford: The Clarendon Press, 1961.
2. Ackerman JJH, Grove TH, Wong GG, Gadian DG, Radda GK. Mapping of metabolites in whole animals by ^{31}P NMR using surface coils. Nature 1980;283:167-170.
3. Albers GW. Expanding the window for thrombolytic therapy in acute stroke. Stroke 1999;30:2230-2237.
4. Allen K, Busza AL, Crockard HA, Frackowiak RS, Gadian DG, Proctor E, Russell RW, Williams SR. Acute cerebral ischaemia: concurrent changes in cerebral blood flow, energy metabolites, pH, and lactate measured with hydrogen clearance and ^{31}P and ^{1}H nuclear magnetic resonance spectroscopy. III. Changes following ischaemia. J Cereb Blood Flow Metab 1988;8:816-821.
5. Allerhand A, Gutowsky HS. Spin-echo NMR studies of chemical exchange. I. Some general aspects. J Chem Phys 1964;41:2115-2126.
6. An H, Lin W. Quantitative measurements of cerebral blood oxygen saturation using magnetic resonance imaging. J Cereb Blood Flow Metab 2000;20:1225-1236.
7. Andrasko J. Water in agarose gels studied by nuclear magnetic resonance relaxation in the rotating frame. Biophysical Journal 1975;15:1235-1243.
8. Andrews BT, Weinstein PR, Keniry M, Pereira B. Sequential in vivo measurement of cerebral intracellular metabolites with phosphorus-31 magnetic resonance spectroscopy during global cerebral ischemia and reperfusion in rats. Neurosurgery 1987;21:699-708.
9. Astrup J, Siesjö BK, Symon L. Thresholds in cerebral ischemia: the ischemic penumbra. Stroke 1981;12:723-725.
10. Avery S, Crockard HA, Ross Russell R. Evolution and resolution of oedema following severe temporary cerebral ischaemia in the gerbil. J Neurol Neurosurg Psych 1984;47:604-610.
11. Ay H, Buonanno FS, Rordorf G, Schaefer PW, Scwamm LH, Wu O, Gonzales RG, Yamada K, Sørensen AG, Koroshetz WJ. Normal diffusion-weighted MRI during stroke-like deficits. Neurology 1999;52:1784-1792.
12. Baird AE, Warach S. Magnetic resonance imaging of acute stroke. J Cereb Blood Flow Metab 1998;18:583-609.
13. Baird AE, Warach S. Imaging developing brain infarction. Curr Opin Neurol 1999;12:65-71.
14. Basser PJ, Mattiello J, Le Bihan D. MR diffusion tensor spectroscopy and imaging. Biophys J 1994;66:259-267.
15. Basser PJ, Pierpaoli C. Microstructural and physiological features of tissues elucidated by quantitative-diffusion-tensor MRI. J Magn Reson B 1996;111:209-219.
16. Beauchamp NJ, Jr., Barker PB, Wang PY, van Zijl PCM. Imaging of acute cerebral ischemia. Radiology 1999;212:307-324.
17. Beauchamp NJ, Jr., Ulug AM, Passe TJ, van Zijl PCM. MR diffusion imaging in stroke: review and controversies. Radiographics 1998;18:1269-1283.
18. Bell BA, Symon L, Branston NM. CBF and time thresholds for the formation of ischemic cerebral edema, and effect of reperfusion in baboons. J Neurosurg 1985;62:31-41.
19. Benveniste H, Hedlund LW, Johnson GA. Mechanism of detection of acute cerebral ischemia in rats by diffusion-weighted magnetic resonance microscopy. Stroke 1992;23:746-754.
20. Bloch F, Hansen WW, Packard ME. Nuclear induction. Phys Rev 1946;69:127.
21. Bloembergen N, Purcell EM, Pound RV. Relaxation effects in nuclear magnetic resonance absorption. Phys Rev 1948;73:679-712.
22. Bose B, Jones SC, Lorig R, Friel HT, Weinstein M, Little JR. Evolving focal cerebral ischemia in cats: spatial correlation of nuclear magnetic resonance imaging, cerebral blood flow, tetrazolium staining, and histopathology. Stroke 1988;19:28-37.
23. Bottomley PA, Foster TH, Argersinger RE, Pfeifer LM. A review of normal tissue hydrogen NMR relaxation times and relaxation mechanisms from 1-100 MHz: dependence on tissue type, NMR frequency, temperature, species, excision, and age. Med Phys 1984;11:425-448.

24. Brooks RA, Battocletti JHS, Sances AJ, Larson SJ, Bowman RL, Kudravcev V. Nuclear magnetic relaxation in blood. IEEE T Bio-Med Eng 1975;BME-22:12-18.
25. Brooks RA, Di Chiro G. Magnetic resonance imaging of stationary blood: A review. Med Phys 1987;14:903-913.
26. Brown AW, Brierley JB. The earliest alterations in rat neurones and astrocytes after anoxia-ischaemia. Acta Neuropathol 1973;23:9-22.
27. Brown III RD, Koenig SH. $1/T_{1\rho}$ and low-field $1/T_1$ of tissue water protons arise from magnetization transfer to macromolecular solid-state broadened lines. Magn Reson Med 1992;28:145-152.
28. Bryant RG. The dynamics of water-protein interactions. Annu Rev Biophys Biomol Struct 1996;25:29-53.
29. Bryant RG, Marill K, Blackmore C, Francis C. Magnetic relaxation in blood and blood clots. Magn Reson Med 1990;13:133-144.
30. Buonanno FS, Pykett IL, Brady TJ, Vielma J, Burt CT, Goldman MR, Hinshaw WS, Pohost GM, Kistler JP. Proton NMR imaging in experimental ischemic infarction. Stroke 1983;14:178-184.
31. Buonanno FS, Pykett IL, Kistler JP, Vielma J, Brady TJ, Hinshaw WS, Goldman MR, Newhouse JH, Pohost GM. Cranial anatomy and detection of ischemic stroke in the cat by nuclear magnetic resonance imaging. Radiology 1982;143:187-193.
32. Busch E, Hoehn-Berlage M, Eis M, Gyngell ML, Hossman KA. Simultaneous recording of EEG, DC potential and diffusion-weighted NMR imaging during potassium induced cortical spreading depression in rats. NMR Biomed 1995;8:59-64.
33. Busza AL, Allen KL, King MD, van Bruggen N, Williams SR, Gadian DG. Diffusion-weighted imaging studies of cerebral ischemia in gerbils. Potential relevance to energy failure. Stroke 1992;23:1602-1612.
34. Cady EB, D'Souza PC, Penrice J, Lorek A. The estimation of local brain temperature by in vivo ^{1}H magnetic resonance spectroscopy. Magn Reson Med 1995;33:862-867.
35. Calamante F, Lythgoe MF, Pell GS, Thomas DL, King MD, Busza AL, Sotak CH, Williams SR, Ordidge RJ, Gadian DG. Early changes in water diffusion, perfusion, T_1, and T_2 during focal cerebral ischemia in the rat studied at 8.5 T. Magn Reson Med 1999;41:479-485.
36. Calamante F, Thomas DL, Pell GS, Wiersma J, Turner R. Measuring cerebral blood flow using magnetic resonance imaging techniques. J Cereb Blood Flow Metab 1999;19:701-735.
37. Carano RA, Li F, Irie K, Helmer KG, Silva MD, Fisher M, Sotak CH. Multispectral analysis of the temporal evolution of cerebral ischemia in the rat brain. J Magn Reson Imaging 2000;12:842-858.
38. Carr HY, E.M. P. Effects of diffusion on free precession in nuclear magnetic resonance experiments. Phys Rev 1954;94:630-638.
39. Chen JC, Hardy PA, Clauberg M, Joshi JG, Parravano J, Deck JH, Henkelman RM, Becker LE, Kucharczyk W. T_2 values in the human brain: comparison with quantitative assays of iron and ferritin. Radiology 1989;173:521-526.
40. Chiarotti G, Cristiani G, Giulotto L. Proton relaxation in pure liquids and in liquids containing paramagnetic gases in solution. Il Nuovo Cimento 1955;I:863-873.
41. Crockard A, Iannotti F, Hunstock AT, Smith RD, Harris RJ, Symon L. Cerebral blood flow and edema following carotid occlusion in the gerbil. Stroke 1980;11:494-498.
42. Crockard HA, Gadian DG, Frackowiak RS, Proctor E, Allen K, Williams SR, Russell RW. Acute cerebral ischaemia: concurrent changes in cerebral blood flow, energy metabolites, pH, and lactate measured with hydrogen clearance and ^{31}P and ^{1}H nuclear magnetic resonance spectroscopy. II. Changes during ischaemia. J Cereb Blood Flow Metab 1987;7:394-402.
43. Davis D, Ulatowski J, Eleff S, Izuta M, Mori S, Shungu D, van Zijl PC. Rapid monitoring of changes in water diffusion coefficients during reversible ischemia in cat and rat brain. Magn Reson Med 1994;31:454-460.
44. Davis TL, Kwong KK, Weisskoff RM, Rosen BR. Calibrated functional MRI: Mapping the dynamics of oxidative metabolism. Proc Natl Acad Sci USA 1998;95:1834-1839.

45. de Crespigny A, Röther J, van Bruggen N, Beaulieu C, Moseley ME. Magnetic resonance imaging assessment of cerebral hemodynamics during spreading depression in rats. J Cereb Blood Flow Metab 1998;18:1008-1017.
46. de Crespigny AJ, Röther J, Beaulieu C, Moseley ME, Hoehn M. Rapid monitoring of diffusion, DC potential, and blood oxygenation changes during global ischemia. Effects of hypoglycemia, hyperglycemia, and TTX. Stroke 1999;30:2212-2222.
47. de Crespigny AJ, Röther J, Beaulieu C, Neumann-Haefelin T, Moseley ME. Comparison of diffusion, blood oxygenation, and blood volume changes during global ischemia in rats. Magn Reson Med 2001;45:10-16.
48. de Crespigny AJ, Wendland MF, Derugin N, Kozniewska E, Moseley ME. Real-time observation of transient focal ischemia and hyperemia in cat brain. Magn Reson Med 1992;27:391-397.
49. de Graaf RA, Braun KP, Nicolay K. Single-shot diffusion trace ^{1}H NMR spectroscopy. Magn Reson Med 2001;45:741-748.
50. Decanniere C, Eleff S, Davis D, van Zijl PC. Correlation of rapid changes in the average water diffusion constant and the concentrations of lactate and ATP breakdown products during global ischemia in cat brain. Magn Reson Med 1995;34:343-352.
51. Deichmann R, Haase A. Quantification of T_1 Values by SNAPSHOT-FLASH NMR Imaging. J Magn Reson 1992;96:608-612.
52. Detre JA, Leigh JS, Williams DS, Koretsky AP. Perfusion imaging. Magn Reson Med 1992;23:37-45.
53. Dickinson RJ, Hall AS, Hind AJ, Young IR. Measurement of changes in tissue temperature using MR imaging. J Comput Assist Tomogr 1986;10:468-472.
54. Diegel JG, Pintar MM. Origin of the nonexponentiality of the water proton spin relaxations in tissue. Biophys J 1975;15:855-860.
55. Dijkhuizen RM, de Graaf RA, Tulleken KA, Nicolay K. Changes in the diffusion of water and intracellular metabolites after excitotoxic injury and global ischemia in neonatal rat brain. J Cereb Blood Flow Metab 1999;19:341-349.
56. Does MD, Zhong J, Gore JC. In vivo measurement of ADC change due to intravascular susceptibility variation. Magn Reson Med 1999;41:236-40.
57. Donahue KM, Weisskoff RM, Burstein D. Water diffusion and exchange as they influence contrast enhancement. J Magn Reson Imaging 1997;7:102-110.
58. Duong TQ, Ackerman JJ, Ying HS, Neil JJ. Evaluation of extra- and intracellular apparent diffusion in normal and globally ischemic rat brain via ^{19}F NMR. Magn Reson Med 1998;40:1-13.
59. Duvvuri U, Goldberg AD, Kranz JK, Hoang L, Reddy R, Wehrli FW, Wand AJ, Englander SW, Leigh JS. Water magnetic relaxation dispersion in biological systems: The contribution of proton exchange and implications for the noninvasive detection of cartilage degradation. Proc Natl Acad Sci U S A 2001;98:12479-12484.
60. Edelman RR, Siewert B, Darby DG, Thangaraj V, Nobre AC, Mesulam MM, Warach S. Qualitative mapping of cerebral blood flow and functional localization with echo-planar MR imaging and signal targeting with alternating radio frequency. Radiology 1994;192:513-520.
61. Edzes HT, Samulski ET. The measurement of cross-relaxation effects in the proton NMR spin-lattice relaxation of water in biological systems: hydrated collagen and muscle. J Magn Res 1978;31:207-229.
62. Engelhardt RT, Johnson GA. $T_{1\rho}$ relaxation and its application to MR histology. Magn Reson Med 1996;35:781-786.
63. Ernst RR, Bodenhausen G, Wokaun A. Principles of Nuclear Magnetic Resonance in One and Two Dimensions. Oxford: Oxford University Press, 1991.
64. Ewing JR, Jiang Q, Boska M, Zhang ZG, Brown SL, Li GH, Divine GW, Chopp M. T_1 and magnetization transfer at 7 Tesla in acute ischemic infarct in the rat. Magn Reson Med 1999;41:696-705.

65. Fatouros PP, Marmarou A, Kraft KA, Inao S, Schwarz FP. In vivo brain water determination by T_1 measurements: effect of total water content, hydration fraction, and field strength. Magn Reson Med 1991;17:402-413.
66. Finch ED, Homer LD. Proton nuclear magnetic resonance relaxation measurements in frog muscle. Biophys J 1974;14:907-921.
67. Fisher M. Characterizing the target of acute stroke therapy. Stroke 1997;28:866-872.
68. Forsen S, Hoffman RA. Study of moderately rapid chemical exchange reactions by means of nuclear magnetic double resonance. J Chem Phys 1963;39:2892-2901.
69. Frahm J, Merboldt KD, Hänicke W, Haase A. Stimulated echo imaging. J Magn Reson 1985;64:81-93.
70. Fullerton GD. Physiological basis of magnetic relaxation. In: Stark DD, Bradley WG, editors. Magn Reson Imaging. Baltimore: Mosby; 1992.
71. Fullerton GD, Potter JL, Dornbluth NC. NMR relaxation of protons in tissues and other macromolecular water solutions. Magn Reson Imaging 1982;1:209-226.
72. Gadian DG. NMR and its applications to living systems, 2nd edition. Oxford: Oxford Science Publications, 1995.
73. Gadian DG, Frackowiak RS, Crockard HA, Proctor E, Allen K, Williams SR, Russell RW. Acute cerebral ischaemia: concurrent changes in cerebral blood flow, energy metabolites, pH, and lactate measured with hydrogen clearance and ^{31}P and ^{1}H nuclear magnetic resonance spectroscopy. I. Methodology. J Cereb Blood Flow Metab 1987;7:199-206.
74. Garwood M, DelaBarre L. The return of the frequency sweep: Designing adiabatic pulses for contemporary NMR. J Magn Reson 2001;153:155-177.
75. Gasparovic C, Matwiyoff NA. The magnetic properties and water dynamics of the red blood cell: a study by proton-NMR lineshape analysis. Magn Reson Med 1992;26:274-299.
76. Gillis P, Peto S, Moiny F, Mispelter J, Cuenod CA. Proton transverse nuclear magnetic relaxation in oxidized blood: a numerical approach. Magn Reson Med 1995;33:93-100.
77. Ginsberg MD. The new language of cerebral ischemia. Am J Neuroradiol 1997;18:1435-1445.
78. Golay X, Silvennoinen MJ, Zhou J, Kauppinen RA, Pekar JJ, van Zijl PCM. Measurement of tissue oxygen extraction ratios from venous blood T_2: Increased precision and validitation of principle. Magn Reson Med 2001;46:282-291.
79. Gowan B. Nuclear magnetic resonance and relaxation. Cambridge: Cambridge University Press, 1997.
80. Grad J, Bryant RG. Nuclear magnetic cross-relaxation spectroscopy. J Magn Reson 1990;90:1-8.
81. Grad J, Mendelson D, Hyder F, Bryant RG. Applications of nuclear magnetic cross-relaxation spectroscopy to tissues. Magn Reson Med 1991;17:452-459.
82. Graves MJ. Magnetic resonance angiography. Br J Radiol 1997;70:6-28.
83. The National Institute of Neurological Disorders and Stroke rt-PA Stroke Study Group. Tissue plasminogen activator for acute ischemic stroke. N Engl J Med 1995;333:1581-1587.
84. Grubb RLJ, Raichel ME, Eichling JO, Ter-Pogossian MM. The effects of changes in $PaCO_2$ on cerebral blood volume, blood flow, and vascular mean transit time. Stroke 1974;5:630-639.
85. Grüne M, van Dorsten FA, Schwindt W, Olah L, Hoehn M. Quantitative T_2* and T_2' maps during reversible focal cerebral ischemia in rats: Separation of blood oxygenation from nonsusceptibility-based contributions. Magn Reson Med 1999;42:1027-1032.
86. Gröhn OHJ, Kauppinen RA. Assessment of brain tissue viability in acute ischemic stroke by BOLD MRI. NMR Biomed 2001;14:432-440.
87. Gröhn OHJ, Kettunen MI, Mäkelä HI, Penttonen M, Pitkänen A, Lukkarinen JA, Kauppinen RA. Early detection of irreversible cerebral ischemia in the rat using dispersion of the magnetic resonance imaging relaxation time, $T_{1\rho}$. J Cereb Blood Flow Metab 2000;20:1457-1466.
88. Gröhn OHJ, Kettunen MI, Penttonen M, Oja JM, van Zijl PCM, Kauppinen RA. Graded reduction of cerebral blood flow in rat as detected by the nuclear magnetic resonance relaxation time T_2: a theoretical and experimental approach. J Cereb Blood Flow Metab 2000;20:316-326.

89. Gröhn OHJ, Lukkarinen JA, Oja JME, van Zijl PCM, Ulatowski JA, Traystman RJ, Kauppinen RA. Noninvasive detection of cerebral hypoperfusion and reversible ischemia from reductions in the magnetic resonance imaging relaxation time, T_2. J Cereb Blood Flow Metab 1998;18:911-920.
90. Gröhn OHJ, Lukkarinen JA, Silvennoinen MJ, Pitkänen A, van Zijl PCM, Kauppinen RA. Quantitative magnetic resonance imaging assessment of cerebral ischemia in rat using on-resonance T_1 in the rotating frame. Magn Reson Med 1999;42:268-276.
91. Grösch L, Noack F. NMR relaxation investigation of water mobility in aqueous bovine serum albumin solutions. Biochim Biophys Acta 1976;453:218-232.
92. Haacke EM, Brown RW, Thompson MR, Venkatesan R. Magnetic resonance imaging : Physical Principles and Sequence Design. New York: John Wiley & Sons, 1999.
93. Hahn EL. Spin echoes. Phys Rev 1950;80:580-594.
94. Hakim AM, Hogan MJ, Carpenter S. Time course of cerebral blood flow and histological outcome after focal cerebral ischemia in rats. Stroke 1992;23:1138-1144.
95. Hakim AM, Shoubridge EA. Cerebral acidosis in focal ischemia. Cerebrovasc Brain Metab Rev 1989;1:115-132.
96. Hakumäki JM, Pirttilä T-RM, Kauppinen RA. Reduction in water and metabolite apparent diffusion coefficients during energy failure involves cation-dependent mechanisms. A nuclear magnetic resonance study of rat cortical brain slices. J Cereb Blood Flow Metab 2000;20:405-411.
97. Halle B. Water in biological systems: the NMR picture. In: Bellisent-Funel M-C, editor Hydration Processes in Biology. Amsterdam: IOS Press; 1999.
98. Hamberg LM, Boccalini P, Stranjalis G, Hunter GJ, Huang Z, Halpern E, Weisskoff RM, Moskowitz MA, Rosen BR. Continuous assessment of relative cerebral blood volume in transient ischemia using steady state susceptibility-contrast MRI. Magn Reson Med 1996;35:168-173.
99. Hamberg LM, McFarlane R, Tasdemiroglu E, Boccalini P, Hunter GJ, Belliveau JW, Moskowitz MA, Rosen BR. Measurement of cerebrovascular changes in cats after transient ischemia using dynamic magnetic resonance imaging. Stroke 1993;24:444-451.
100. Hansen AJ. The extracellular potassium concentration in brain cortex following ischemia in hypo- and hyperglycemic rats. Acta Physiol Scand 1978;102:324-329.
101. Hansen AJ, Olsen CE. Brain extracellular space during spreading depression and ischemia. Acta Physiol Scand 1980;108:355-365.
102. Hansen AJ, Zeuthen T. Extracellular ion concentrations during spreading depression and ischemia in the rat brain cortex. Acta Physiol Scand 1981;113:437-445.
103. Harris NG, Zilkha E, Houseman J, Symms MR, Obrenovitch TP, Williams SR. The relationship between the apparent diffusion coefficient measured by magnetic resonance imaging, anoxic depolarization, and glutamate efflux during experimental cerebral ischemia. J Cereb Blood Flow Metab 2000;20:28-36.
104. Heiss WD, Hayakawa T, Waltz AG. Cortical neuronal function during ischemia. Effects of occlusion of one middle cerebral artery on single-unit activity in cats. Arch Neurol 1976;33:813-820.
105. Henkelman RM, Huang X, Xiang QS, Stanisz GJ, Swanson SD, Bronskill MJ. Quantitative interpretation of magnetization transfer. Magn Reson Med 1993;29:759-766.
106. Henkelman RM, Stanisz GJ, Graham SJ. Magnetization transfer in MRI: a review. NMR Biomed 2001;14:57-64.
107. Hoehn M, Nicolay K, Franke C, van der Sanden B. Application of magnetic resonance to animal models of cerebral ischemia. J Magn Reson Imaging 2001;14:491-509.
108. Hoehn-Berlage M, Eis M, Back T, Kohno K, Yamashita K. Changes of relaxation times (T_1, T_2) and apparent diffusion coefficient after permanent middle cerebral artery occlusion in the rat: temporal evolution, regional extent, and comparison with histology. Magn Reson Med 1995;34:824-834.
109. Hoehn-Berlage M, Norris DG, Kohno K, Mies G, Leibfritz D, Hossmann KA. Evolution of regional changes in apparent diffusion coefficient during focal ischemia of rat brain: the

relationship of quantitative diffusion NMR imaging to reduction in cerebral blood flow and metabolic disturbances. J Cereb Blood Flow Metab 1995;15:1002-1011.
110. Horikawa Y, Naruse S, Tanaka C, Hirikawa K, Nishikawa H. Proton NMR relaxation times in ischemic brain edema. Stroke 1986;17:1149-1152.
111. Hossmann KA. Viability thresholds and the penumbra of focal ischemia. Ann Neurol 1994;36:557-565.
112. Hossmann KA. Reperfusion of the brain after global ischemia: hemodynamic disturbances. Shock 1997;8:95-103.
113. Hossmann KA, Fischer M, Bockhorst K, Hoehn-Berlage M. NMR imaging of the apparent diffusion coefficient (ADC) for the evaluation of metabolic suppression and recovery after prolonged cerebral ischemia. J Cereb Blood Flow Metab 1994;14:723-731.
114. Hossmann KA, Sakaki S, Kimoto K. Cerebral uptake of glucose and oxygen in the cat brain after prolonged ischemia. Stroke 1976;7:301-305.
115. Hossmann KA, Schuier FJ. Experimental brain infarcts in cats. I. Pathophysiological observations. Stroke 1980;11:583-592.
116. Huang NC, Yongbi MN, Helpern JA. The influence of preischemic hyperglycemia on acute changes in the apparent diffusion coefficient of brain water following global ischemia in rats. Brain Res 1997;757:139-145.
117. Huang NC, Yongbi MN, Helpern JA. The influence of preischemic hyperglycemia on acute changes in brain water ADCw following focal ischemia in rats. Brain Res 1998;788:137-143.
118. Jenkins LW, Povlishock JT, Becker DP, Miller JD, Sullivan HG. Complete cerebral ischemia. An ultrastructural study. Acta Neuropathol (Berl) 1979;48:113-125.
119. Jezzard P, Matthews PM, Smith SM. Functional MRI - An Introduction to Methods. Oxford: Oxford University Press, 2001.
120. Jones GP. Spin-lattice relaxation in the rotating frame: weak-collision case. Phys Rev 1966;148:332-335.
121. Kamman RL, Go KG, Brouwer W, Berendsen HJ. Nuclear magnetic resonance relaxation in experimental brain edema: effects of water concentration, protein concentration, and temperature. Magn Reson Med 1988;6:265-274.
122. Kato H, Kogure K, Ohtomo H, Izumiyama M, Tobita M, Matsui S, Yamamoto E, Kohno H, Ikebe Y, Watanabe T. Characterization of experimental ischemic brain edema utilizing proton nuclear magnetic resonance imaging. J Cereb Blood Flow Metab 1986;6:212-221.
123. Kato H, Kogure K, Ohtomo H, Tobita M, Matsui S, Yamamoto E, Kohno H. Correlations between proton nuclear magnetic resonance imaging and retrospective histochemical images in experimental cerebral infarction. J Cereb Blood Flow Metab 1985;5:267-274.
124. Katsura K, Asplund B, Ekholm A, Siesjö BK. Extra- and intracellular pH in the brain during ischaemia, related to tissue lactate content in normo- and hypercapnic rats. Eur J Neurosci 1992;4:166-176.
125. Kavec M, Gröhn OHJ, Kettunen MI, Silvennoinen MJ, Penttonen M, Kauppinen RA. Use of spin echo T_2 BOLD in assessment of cerebral misery perfusion at 1.5 T. MAGMA 2001;12:32-39.
126. Kidwell CS, Alger JR, Di Salle F, Starkman S, Villablanca P, Bentson J, Saver JL. Diffusion MRI in patients with transient ischemic attacks. Stroke 1999;30:1174-1180.
127. Kim SG. Quantification of relative cerebral blood flow change by flow-sensitive alternating inversion recovery (FAIR) technique: application to functional mapping. Magn Reson Med 1995;34:293-301.
128. Knight RA, Dereski MO, Helpern JA, Ordidge RJ, Chopp M. Magnetic resonance imaging assessment of evolving focal cerebral ischemia. Comparison with histopathology in rats. Stroke 1994;25:1252-1262.
129. Knijn A, de Beer R, van Ormondt D. Frequency-selective quantification in the time domain. J Magn Reson 1992;97:444-450.

130. Knispel RR, Thompson RT, Pintar MM. Dispersion of proton spin-lattice relaxation in tissues. J Magn Reson 1974;14:44-51.
131. Koenig SH, Brown III RD. Relaxometry and the source of contrast in MRI. In: Gillies RJ, editor NMR in physiology and biomedicine. San Diego, USA: Academic Press; 1994.
132. Koenig SH, Brown RD. A molecular theory of relaxation and magnetization transfer: application to cross-linked BSA, a model for tissue. Magn Reson Med 1993;30:685-695.
133. Kogure K, Busto R, Scheinberg P, Reinmuth OM. Energy metabolites and water content in rat brain during the early stage of development of cerebral infarction. Brain 1974;97:103-114.
134. Kwong KK, Chesler DA, Weisskoff RM, Donahue KM, Davis TL, Østergaard L, Campbell TA, Rosen BR. MR perfusion studies with T_1-weighted echo planar imaging. Magn Reson Med 1995;34:878-887.
135. Kågström E, Smith ML, Siesjö BK. Local cerebral blood flow in the recovery period following complete cerebral ischemia in the rat. J Cereb Blood Flow Metab 1983;3:170-182.
136. Lansberg MG, Thijs VN, O'Brien MW, Ali JO, de Crespigny AJ, Tong DC, Moseley ME, Albers GW. Evolution of apparent diffusion coefficient, diffusion-weighted, and T_2-weighted signal intensity of acute stroke. Am J Neuroradiol 2001;22:637-644.
137. Lassen NA. The luxury-perfusion syndrome and its possible relation to acute metabolic acidosis localised within the brain. Lancet 1966;2:1113-1115.
138. Le Bihan D. Diffusion and perfusion magnetic resonance imaging. New York: Raven Press, 1995.
139. Le Bihan D, Breton E, Lallemand D, Grenier P, Cabanis E, Laval-Jeantet M. MR imaging of intravoxel incoherent motions: application to diffusion and perfusion in neurologic disorders. Radiology 1986;161:401-407.
140. Le Bihan D, Mangin JF, Poupon C, Clark CA, Pappata S, Molko N, Chabriat H. Diffusion tensor imaging: concepts and applications. J Magn Reson Imaging 2001;13:534-546.
141. Levy DE, Duffy TE. Cerebral energy metabolism during transient ischemia and recovery in the gerbil. J Neurochem 1977;28:63-70.
142. Li F, Han SS, Tatlisumak T, Liu KF, Garcia JH, Sotak CH, Fisher M. Reversal of acute apparent diffusion coefficient abnormalities and delayed neuronal death following transient focal cerebral ischemia in rats. Ann Neurol 1999;46:333-342.
143. Li F, Liu KF, Silva MD, Omae T, Sotak CH, Fenstermacher JD, Fisher M, Hsu CY, Lin W. Transient and permanent resolution of ischemic lesions on diffusion-weighted imaging after brief periods of focal ischemia in rats : correlation with histopathology. Stroke 2000;31:946-954.
144. Li F, Silva MD, Sotak CH, Fisher M. Temporal evolution of ischemic injury evaluated with diffusion-, perfusion-, and T_2-weighted MRI. Neurology 2000;54:689-696.
145. Liepinsh E, Otting G. Proton exchange rates from amino acid side chains-implications for image contrast. Magn Reson Med 1996;35:30-42.
146. Lin W, Lee J-M, Vo KD, An H, Celik A, Lee Y, Hsu CY. Clinical utility of $CMRO_2$ obtained with MRI in determining ischemic brain tissue at risk. Stroke 2001;32:341-342.
147. Lin W, Paczynski RP, Venkatesan R, He YY, Powers WJ, Hsu CY, Haacke EM. Quantitative regional brain water measurement with magnetic resonance imaging in a focal ischemia model. Magn Reson Med 1997;38:303-310.
148. Lindsberg PJ, Roine RO, Tatlisumak T, Sairanen T, Kaste M. The future of stroke treatment. Neurol Clin 2000;18:495-510.
149. Lipton P. Ischemic cell death in brain neurons. Physiol Rev 1999;79:1431-1568.
150. Liu KF, Li F, Tatlisumak T, Garcia JH, Sotak CH, Fisher M, Fenstermacher JD. Regional variations in the apparent diffusion coefficient and the intracellular distribution of water in rat brain during acute focal ischemia. Stroke 2001;32:1897-1905.
151. Ljunggren B, Schutz H, Siesjö BK. Changes in energy state and acid-base parameters of the rat brain during complete compression ischemia. Brain Res 1974;73:277-289.
152. Longa EZ, Weinstein PR, Carlson S, Cummins R. Reversible middle cerebral artery occlusion without craniectomy in rats. Stroke 1989;20:84-91.

153. Look DC, Lowe IJ. Nuclear magnetic dipole-dipole relaxation along the static and rotating magnetic fields: application to gypsum. J Chem Phys 1966;44:2995-3000.
154. Lorek A, Takei Y, Cady EB, Wyatt JS, Penrice J, Edwards AD, Peebles D, Wylezinska M, Owenreece H, Kirkbride V, Cooper CE, Aldridge RF, Roth SC, Brown G, Delpy DT, Reynolds EOR. Delayed ("secondary") cerebral energy failure after acute hypoxia-ischemia in the newborn piglet: Continuous 48-hour studies by phosphorus magnetic resonance spectroscopy. Pediatr Res 1994;36:699-706.
155. Lythgoe MF, Thomas DL, Calamante F, Pell GS, King MD, Busza AL, Sotak CH, Williams SR, Ordidge RJ, Gadian DG. Acute changes in MRI diffusion, perfusion, T_1, and T_2 in a rat model of oligemia produced by partial occlusion of the middle cerebral artery. Magn Reson Med 2000;44:706-712.
156. Ma J, Wehrli FW. Method for image-based measurement of the reversible and irreversible contribution to the transverse-relaxation rate. J Magn Reson B 1996;111:61-69.
157. Mano I, Levy RM, Crooks LE, Hosobuchi Y. Proton nuclear magnetic resonance imaging of acute experimental cerebral ischemia. Invest Radiol 1983;18:345-351.
158. Martin RM, Halsey JH, Reneau DD. A critical evaluation of oxygen disappearance during stop flow in the gerbil brain. Neurol Res 1982;4:21-34.
159. Menon RS, Allen PS. Solvent proton relaxation of aqueous solutions of the serum proteins α2-macroglobulin, fibrinogen, and albumin. Biophys J 1990;57:389-396.
160. Mies G, Ishimaru S, Xie Y, Seo K, Hossmann KA. Ischemic thresholds of cerebral protein synthesis and energy state following middle cerebral artery occlusion in rat. J Cereb Blood Flow Metab 1991;11:753-761.
161. Minematsu K, Li L, Sotak CH, Davis MA, Fisher M. Reversible focal ischemic injury demostrated by diffusion-weighted magnetic resonance imaging in rats. Stroke 1992;23:1304-1311.
162. Mintorovitch J, Moseley ME, Chileuitt L, Shimizu H, Cohen Y, Weinstein PR. Comparison of diffusion- and T_2-weighted MRI for the early detection of cerebral ischemia and reperfusion in rats. Magn Reson Med 1991;18:39-50.
163. Mintorovitch J, Yang GY, Shimizu H, Kucharczyk J, Chan PH, Weinstein PR. Diffusion-weighted magnetic resonance imaging of acute focal cerebral ischemia: comparison of signal intensity with changes in brain water and Na^+,K^+-ATPase activity. J Cereb Blood Flow Metab 1994;14:332-336.
164. Moonen CTW, Bandettini PA. Functional MRI. Berlin: Springer Verlag, 1999.
165. Mori S, Crain BJ, Chacko VP, van Zijl PC. Three-dimensional tracking of axonal projections in the brain by magnetic resonance imaging. Ann Neurol 1999;45:265-269.
166. Mori S, Eleff SM, Pilatus U, Mori N, van Zijl PCM. Proton NMR spectroscopy of solvent saturable resonances: A new approach to study pH effects *in situ*. Magn Reson Med 1998;40:36-42.
167. Mori S, van Zijl PC. Diffusion weighting by the trace of the diffusion tensor within a single scan. Magn Reson Med 1995;33:41-52.
168. Moseley ME, Cohen Y, Mintorovitch J, Chileuitt L, Shimizu H, Kucharczyk J, Wendland MF, Weinstein PR. Early detection of regional cerebral ischemia in cats: comparison of diffusion- and T_2-weighted MRI and spectroscopy. Magn Reson Med 1990;14:330-346.
169. Moseley ME, Wendland MF, Kucharczyk J. Magnetic resonance imaging of diffusion and perfusion. Top Magn Reson Imaging 1991;3:50-67.
170. Mrsulja BB, Djuricic BM, Cvejic V, Mrsulja BJ, Abe K, Spatz M, Klatzo I. Biochemistry of experimental ischemic brain edema. Adv Neurol 1980;28:217-230.
171. Mulkern RV, Patz S, Brooks M, Metcalf DC, Jolesz FA. Spin-lock techniques and CPMG imaging sequences: a critical appraisal of $T_{1\rho}$ contrast at 0.15 T. Magn Reson Imaging 1989;7:437-444.
172. Mäkelä HI, Gröhn OHJ, Kettunen MI, Kauppinen RA. Proton exchange as a relaxation mechanism for T_1 in the rotating frame in native and immobilized protein solutions. Biochem Biophys Res Commun 2001;289:813-818.

173. Mäkelä HI, Kettunen MI, Gröhn OHJ, Kauppinen RA. Quantitative $T_{1\rho}$ and magnetization transfer MRI of acute cerebral ischaemia in the rat. J Cereb Blood Flow Metab 2002;22:547-558.
174. Nair PK, Buerk DG, Halsey JH, Jr. Comparisons of oxygen metabolism and tissue PO_2 in cortex and hippocampus of gerbil brain. Stroke 1987;18:616-622.
175. Naressi A, Couturier C, Devos JM, Janssen M, Mangeat C, de Beer R, Graveron-Demilly D. Java-based graphical user interface for the MRUI quantitation package. MAGMA 2001;12:141-152.
176. Naruse S, Horikawa Y, Tanaka C, Hirakawa K, Nishikawa H, Watari H. In vivo measurement of energy metabolism and the concomitant monitoring of electroencephalogram in experimental cerebral ischemia. Brain Res 1984;296:370-372.
177. Naruse S, Horikawa Y, Tanaka C, Hirakawa K, Nishikawa H, Yoshizaki K. Significance of proton relaxation time measurement in brain edema, cerebral infarction and brain tumors. Magn Reson Imaging 1986;4:293-304.
178. Neil JJ, Duong TQ, Ackerman JJH. Evaluation of intracellular diffusion in normal and globally-ischemic rat brain via ^{133}Cs NMR. Magn Reson Med 1996;35:329-335.
179. Nekolla S, Gneiting T, Syha J, Deichmann R, Haase A. T_1 maps by K-space reduced snapshot-FLASH MRI. J Comput Assist Tomogr 1992;16:327-332.
180. Nemoto EM, Hossmann KA, Cooper HK. Post-ischemic hypermetabolism in cat brain. Stroke 1981;12:666-676.
181. Neumann-Haefelin T, Moseley ME, Albers GW. New magnetic resonance imaging methods for cerebrovascular disease: emerging clinical applications. Ann Neurol 2000;47:559-570.
182. Newberg Milde L. Pathophysiology of ischemic brain injury. Crit Care Clin 1989;5:729-753.
183. Nicholson C, Sykova E. Extracellular space structure revealed by diffusion analysis. Trends Neurosci 1998;21:207-215.
184. Ogawa S, Lee TM, Kay AR, Tank DW. Brain magnetic resonance imaging with contrast dependent on blood oxygenation. Proc Natl Acad Sci U S A 1990;87:9868-9872.
185. Ogawa S, Lee T-M, Nayak AS, Glynn P. Oxygenation-sensitive contrast in magnetic resonance image of rodent brain at high magnetic fields. Magn Reson Med 1990;14:68-78.
186. Ogawa S, Menon RS, Tank DW, Kim S-G, Merkle H, Ellerman JM, Ugurbil K. Functional brain mapping by blood oxygenation level-dependent contrast magnetic resonance imaging: A comparison of signal characteristics with a biophysical model. Biophys J 1993;64:803-812.
187. Oja JME, Gillen JS, Kauppinen RA, Kraut M, van Zijl PCM. Determination of oxygen extraction ratios by magnetic resonance imaging. J Cereb Blood Flow Metab 1999;19:1289-1295.
188. Olah L, Wecker S, Hoehn M. Relation of apparent diffusion coefficient changes and metabolic disturbances after 1 hour of focal cerebral ischemia and at different reperfusion phases in rats. J Cereb Blood Flow Metab 2001;21:430-439.
189. Olesen J, Paulson OB, Lassen NA. Regional cerebral blood flow in man determined by the initial slope of the clearance of intra-arterially injected ^{133}Xe. Stroke 1971;2:519-540.
190. Ordidge RJ, Helpern JA, Knight RA, Qing ZX, Welch KM. Investigation of cerebral ischemia using magnetization transfer contrast (MTC) MR imaging. Magn Reson Imaging 1991;9:895-902.
191. Ostroff ED, Waugh JS. Multiple spin echoes and spin locking in solids. Phys Rev Lett 1966;16:1097-1098.
192. Otting G. NMR studies of water bound to biological molecules. J Prog NMR Spectr 1997;31:259-285.
193. Paulson OB, Hertz MM, Bolwig TG, Lassen NA. Water filtration and diffusion across the blood brain barrier in man. Acta Neurol Scand 1977;64 suppl.:492-493.
194. Payen JF, Vath A, Koenigsberg B, Bourlier V, Decorps M. Regional cerebral plasma volume response to carbon dioxide using magnetic resonance imaging. Anesthesiology 1998;88:984-992.
195. Pettigrew LC, Holtz ML, Craddock SD, Minger SL, Hall N, Geddes JW. Microtubular proteolysis in focal cerebral ischemia. J Cereb Blood Flow Metab 1996;16:1189-1202.

196. Pfeuffer J, Dreher W, Sykova E, Leibfritz D. Water signal attenuation in diffusion-weighted ^{1}H NMR experiments during cerebral ischemia: influence of intracellular restrictions, extracellular tortuosity, and exchange. Magn Reson Imaging 1998;16:1023-1032.
197. Pierpaoli C, Alger JR, Righini A, Mattiello J, Dickerson R, Des Pres D, Barnett A, Di Chiro G. High temporal resolution diffusion MRI of global cerebral ischemia and reperfusion. J Cereb Blood Flow Metab 1996;16:892-905.
198. Powers WJ. Cerebral hemodynamics in ischemic cerebrovascular disease. Ann Neurol 1991;29:231-240.
199. Pulsinelli WA, Levy DE, Duffy TE. Regional cerebral blood flow and glucose metabolism following transient forebrain ischemia. Ann Neurol 1982;11:499-502.
200. Rehncrona S, Mela L, Siesjö BK. Recovery of brain mitochondrial function in the rat after complete and incomplete cerebral ischemia. Stroke 1979;10:437-446.
201. Rommel E, Kimmich R. $T_{1\rho}$ dispersion imaging and volume-selective $T_{1\rho}$ dispersion weighted NMR spectroscopy. Magn Reson Med 1989;12:390-399.
202. Roussel SA, van Bruggen N, King MD, Gadian DG. Identification of collaterally perfused areas following focal ischemia in the rat by comparison of gradient echo and diffusion-weighted MRI. J Cereb Blood Flow Metab 1995;15:578-586.
203. Roussel SA, van Bruggen N, King MD, Houseman J, Williams SR, Gadian DG. Monitoring the initial expansion of focal ischaemic changes by diffusion-weighted MRI using a remote controlled method of occlusion. NMR Biomed 1994;7:21-28.
204. Rudin M, Beckmann N, Porszasz R, Reese T, Bochelen D, Sauter A. In vivo magnetic resonance methods in pharmaceutical research: current status and perspectives. NMR Biomed 1999;12:69-97.
205. Saini S, Edelman RR, Sharma P, Li W, Mayo-Smith W, Slater GJ, Eisenberg PJ, Hahn PF. Blood-pool MR contrast material for detection and characterization of focal hepatic lesions: initial clinical experience with ultrasmall superparamagnetic iron oxide (AMI-227). Am J Roentgenol 1995;164:1147-1152.
206. Salgado ED, Weinstein M, Furlan AJ, Modic MT, Beck GJ, Estes M, Awad I, Little JR. Proton magnetic resonance imaging in ischemic cerebrovascular disease. Ann Neurol 1986;20:502-507.
207. Sandor P, Cox van Put J, de Jong W, de Wied D. Continuous measurement of cerebral blood volume in rats with the photoelectric technique: effect of morphine and naloxone. Life Sci 1986;39:1657-1665.
208. Santyr GE, Henkelman RM, Bronskill MJ. Variation in measured transverse relaxation in tissue resulting from spin locking with the CPMG sequence. J Magn Reson 1988;79:28-44.
209. Schlaug G, Benfield A, Baird AE, Siewert B, Lövblad KO, Parker RA, Edelman RR, Warach S. The ischemic penumbra: operationally defined by diffusion and perfusion MRI. Neurology 1999;53:1528-1537.
210. Schlaug G, Siewert B, Benfield A, Edelman RR, Warach S. Time course of the apparent diffusion coefficient (ADC) abnormality in human stroke. Neurology 1997;49:113-119.
211. Schwab M, Bauer R, Zwiener U. The distribution of normal brain water content in Wistar rats and its increase due to ischemia. Brain Res 1997;749:82-87.
212. Sepponen R. Rotating frame and magnetization transfer. In: Stark D, Bradley WG, editors. Magnetic Resonance Imaging. Mosby-Year Book; 1986.
213. Sepponen R, Tanttu JI, Suramo I, Sipponen JI, Kaste M. $T_{1\rho}$ and $T_{1\rho}$ dispersion imaging in patients with cerebral infarction. *In:* 5th Annual Meeting of Society of Magnetic Resonance in Medicine, Montreal, Canada, 1986.
214. Sharan M, Jones MDJ, Koehler RC, Traystman RJ, Popel AS. A compartmental model for oxygen transport in brain microcirculation. Ann Biomed Engin 1989;17:13-38.
215. Siesjö BK. Cell damage in the brain: a speculative synthesis. J Cereb Blood Flow Metab 1981;1:155-185.

216. Siesjö BK, Wieloch T. Cerebral metabolism in ischaemia: neurochemical basis for therapy. Br J Anaesth 1985;57:47-62.
217. Sipponen JT, Kaste M, Ketonen L, Sepponen RE, Katevuo K, Sivula A. Serial nuclear magnetic resonance (NMR) imaging in patients with cerebral infarction. J Comput Assist Tomogr 1983;7:585-589.
218. Snyder JV, Nemoto EM, Carroll RG, Safar P. Global ischemia in dogs: intracranial pressures, brain blood flow and metabolism. Stroke 1975;6:21-27.
219. Stejskal EO, Tanner JE. Spin diffusion measurements: spin-echoes in the presence of a time-dependent field gradient. J Chem Phys 1965;42:288-292.
220. Szafer A, Zhong J, Gore JC. Theoretical model for water diffusion in tissues. Magn Reson Med 1995;33:697-712.
221. Sørensen AG, Buonanno FS, Gonzalez RG, Schwamm LH, Lev MH, Huang-Hellinger FR, Reese TG, Weisskoff RM, Davis TL, Suwanwela N, Can U, Moreira JA, Copen WA, Look RB, Finklestein SP, Rosen BR, Koroshetz WJ. Hyperacute stroke: evaluation with combined multisection diffusion-weighted and hemodynamic weighted echo-planar imaging. Radiology 1996;199:391-401.
222. Tadamura E, Hatabu H, Li W, Prasad PV, Edelman RR. Effect of oxygen inhalation on relaxation times in various tissues. J Magn Reson Imaging 1997;7:220-225.
223. Takano K, Latour LL, Formato JE, Carano RA, Helmer KG, Hasegawa Y, Sotak CH, Fisher M. The role of spreading depression in focal ischemia evaluated by diffusion mapping. Ann Neurol 1996;39:308-318.
224. Tamura H, Hatazawa J, Toyoshima H, Shimosegawa E, Okudera T. Detection of deoxygenation-related signal change in acute ischemic stroke patients by T_2*-weighted magnetic resonance imaging. Stroke 2002;33:967-971.
225. Tanner JE. Intracellular diffusion of water. Arch Biochem Biophys 1983;224:416-428.
226. Taylor DJ, Bore PJ, Styles P, Gadian DG, Radda GK. Bioenergetics of intact human muscle. A ^{31}P nuclear magnetic resonance study. Mol Biol Med 1983;1:77-94.
227. Thomas DL, Lythgoe MF, Pell GS, Calamante F, Ordidge RJ. The measurement of diffusion and perfusion in biological systems using magnetic resonance imaging. Phys Med Biol 2000;45:R97-138.
228. Thomas DL, Pell GS, Lythgoe MF, Gadian DG, Ordidge RJ. A quantitative method for fast diffusion imaging using magnetization-prepared TurboFLASH. Magn Reson Med 1998;39:950-960.
229. Thompson RT, Knispel RR, Pintar MM. A study of the proton exchange in tissue water by spin relaxation in the rotating frame. Chem Phys Lett 1973;22:335-337.
230. Thulborn KR, du Boulay GH, Duchen LW, Radda G. A ^{31}P nuclear magnetic resonance in vivo study of cerebral ischaemia in the gerbil. J Cereb Blood Flow Metab 1982;2:299-306.
231. Thulborn KR, Waterton JC, Matthews PM, Radda GK. Oxygenation dependence of the transverse relaxation time of water protons in whole blood at high field. Biochim Biophys Acta 1982;714:265-270.
232. Todd NV, Picozzi P, Crockard HA. Quantitative measurement of cerebral blood flow and cerebral blood volume after cerebral ischaemia. J Cereb Blood Flow Metab 1986;6:338-341.
233. Todd NV, Picozzi P, Crockard HA, Ross Russell RW. Recirculation after cerebral ischemia. Simultaneous measurement of cerebral blood flow, brain edema, cerebrovascular permeability and cortical EEG in the rat. Acta Neurol Scand 1986;74:269-278.
234. Todd NV, Picozzi P, Crockard HA, Russell RR. Reperfusion after cerebral ischemia: influence of duration of ischemia. Stroke 1986;17:460-466.
235. Toole JF. Cerebrovascular Disorders, Fifth edition. Philadelphia: Lippincott, Williams & Wilkins, 1999.
236. Turner R, Le Bihan D, Moonen CTW, Despres D, Frank J. Echo-planar time course MRI of cat brain oxygenation changes. Magn Reson Med 1991;22:159-166.

237. Ulatowski JA, Oja JM, Suarez JI, Kauppinen RA, Traystman RJ, van Zijl PC. In vivo determination of absolute cerebral blood volume using hemoglobin as a natural contrast agent: An MRI study using altered arterial carbon dioxide tension. J Cereb Blood Flow Metab 1999;19:809-817.
238. Ulug AM, Beauchamp NJ, Bryan RN, van Zijl PCM. Absolute quantitation of diffusion constants in human stroke. Stroke 1997;28:483-490.
239. van Bruggen N, Cullen BM, King MD, Doran M, Williams SR, Gadian DG, Cremer JE. T_2- and diffusion-weighted magnetic resonance imaging of a focal ischemic lesion in rat brain. Stroke 1992;23:575-582.
240. van Bruggen N, Roberts TPL, Cremer JE. The application of magnetic resonance imaging to the study of experimental cerebral ischaemia. Cerebrovasc Brain Metab Rev 1994;6:180-210.
241. van den Boogaart A. Magnetic Resonance User Interface (MRUI), v. 96.3 edition: http://mrui-web.uab.es/mrui/mruiHomePage.html, 1997.
242. van der Toorn A, Dijkhuizen RM, Tulleken CA, Nicolay K. Diffusion of metabolites in normal and ischemic rat brain measured by localized ^{1}H MRS. Magn Reson Med 1996;36:914-922.
243. van der Toorn A, Sykova E, Dijkhuizen RM, Vorisek I, Vargova L, Skobisova E, van Lookeren Campagne M, Reese T, Nicolay K. Dynamic changes in water ADC, energy metabolism, extracellular space volume, and tortuosity in neonatal rat brain during global ischemia. Magn Reson Med 1996;36:52-60.
244. van Gelderen P, de Vleeschouwer MHM, DesPres D, Pekar J, van Zijl PCM, Moonen CTW. Water diffusion and acute stroke. Magn Reson Med 1994;31:154-163.
245. van Lookeren Campagne M, Thomas GR, Thibodeaux H, Palmer JT, Williams SP, Lowe DG, van Bruggen N. Secondary reduction in the apparent diffusion coefficient of water, increase in cerebral blood volume, and delayed neuronal death after middle cerebral artery occlusion and early reperfusion in the rat. J Cereb Blood Flow Metab 1999;19:1354-1364.
246. van Lookeren Campagne M, Verheul JB, Nicolay K, Balazs R. Early evolution and recovery from excitotoxic injury in the neonatal rat brain: a study combining magnetic resonance imaging, electrical impedance, and histology. J Cereb Blood Flow Metab 1994;14:1011-1023.
247. van Zijl PC, Eleff SM, Ulatowski JA, Oja JM, Ulug AM, Traystman RJ, Kauppinen RA. Quantitative assessment of blood flow, blood volume and blood oxygenation effects in functional magnetic resonance imaging. Nat Med 1998;4:159-167.
248. Wang PY, Barker PB, Wityk RJ, Ulug AM, van Zijl PCM, Beauchamp NJJ. Diffusion-negative stroke: a report of two cases. Am J Neuroradiol 1999;20:1876-1880.
249. Vanhamme L, van den Boogaart A, Van Huffel S. Improved method for accurate and efficient quantification of MRS data with use of prior knowledge. J Magn Reson 1997;129:35-43.
250. Warach S, Chien D, Li W, Ronthal M, Edelman RR. Fast magnetic resonance diffusion-weighted imaging of acute human stroke. Neurology 1992;42:1717-1723.
251. Watanabe O, West CR, Bremer A. Experimental regional cerebral ischemia in the middle cerebral artery territory in primates. Part 2: Effects on brain water and electrolytes in the early phase of MCA stroke. Stroke 1977;8:71-76.
252. Welch KM, Levine SR, Martin G, Ordidge R, van de Linde AM, Halpern JA. Magnetic resonance spectroscopy in cerebral ischemia. Neurol Clin 1992;10:1-29.
253. Welch KM, Windham J, Knight RA, Nagesh V, Hugg JW, Jacobs M, Peck D, Booker P, Dereski MO, Levine SR. A model to predict the histopathology of human stroke using diffusion and T_2-weighted magnetic resonance imaging. Stroke 1995;26:1983-1989.
254. Welch KMA, Caplan LR, Reis DJ, Siesjö BK, Weir B. Primer on Cerebrovascular Diseases. San Diego, USA: Academic Press, 1997.
255. Venu K, Denisov VP, Halle B. Water ^{1}H magnetic relaxation dispersion in protein solutions. A quantitative assessment of internal hydration, proton exchange, and cross-relaxation. J Am Chem Soc 1997;119:3122-3134.

256. Wick M, Nagatomo Y, Prielmeier F, Frahm J. Alteration of intracellular metabolite diffusion in rat brain in vivo during ischemia and reperfusion. Stroke 1995;26:1930-1933.
257. Williams DS, Detre JA, Leigh JS, Koretsky AP. Magnetic resonance imaging of perfusion using spin inversion of arterial water. Proc Natl Acad Sci U S A 1992;89:212-216.
258. Wolff SD, Balaban RS. Magnetization transfer contrast (MTC) and tissue water proton relaxation in vivo. Magn Reson Med 1989;10:135-144.
259. Wong EC, Cox RW, Song AW. Optimized isotropic diffusion weighting. Magn Reson Med 1995;34:139-143.
260. Wuthrich K. NMR of Proteins and Nucleic Acids. New York: John Wiley & Sons, 1986.
261. Xie Y, Mies G, Hossmann KA. Ischemic threshold of brain protein synthesis after unilateral carotid artery occlusion in gerbils. Stroke 1989;20:620-626.
262. Yablonskiy DA, Haacke EM. Theory of NMR signal behavior in magnetically inhomogeneous tissues: the static dephasing regime. Magn Reson Med 1994;32:749-763.
263. Young W. H_2 clearance measurement of blood flow: a review of technique and polarographic principles. Stroke 1980;11:552-564.
264. Young W, Rappaport ZH, Chalif DJ, Flamm ES. Regional brain sodium, potassium, and water changes in the rat middle cerebral artery occlusion model of ischemia. Stroke 1987;18:751-759.
265. Zhou D, Bryant RG. Magnetization transfer, cross-relaxation, and chemical exchange in rotationally immobilized protein gels. Magn Reson Med 1994;32:725-732.
266. Zhou J, Wilson DA, Ulatowski J, Traystman RJ, van Zijl PCM. Two-compartment exchange model for perfusion quantification using arterial spin tagging. J Cerebral Blood Flow Metab 2001;21:440-455.
267. Zimmerman JR, Brittin WE. Nuclear magnetic resonance studies in multiple phase systems: Lifetime of a water molecule in an adsorbing phase on silica gel. J Phys Chem 1957;61:1328-1333.
268. Østergaard L, Sørensen AG, Kwong KK, Gyldensted C, Weisskoff RM, Rosen BR. High resolution measurement of cerebral blood flow using intravascular tracer bolus passages. Part II: Experimental comparison and preliminary results. Magn Reson Med 1996;36:726-736.
269. Østergaard L, Weisskoff RM, Chesler DA, Gyldensted C, Rosen BR. High resolution measurement of cerebral blood flow using intravascular tracer bolus passages. Part I: Mathematical approach and statistical analysis. Magn Reson Med 1996;36:715-725.

Kuopion yliopiston julkaisuja G. - A.I. Virtanen -instituutti
Kuopio University Publications G. - A.I. Virtanen Institute for Molecular Sciences

1. **Kontkanen, Outi.** Gene expression in rat brain: alterations by antipsychotic drugs. 2002. 88 p. + appendix. Diss. 20 €